Supplementary Data for

Condensate-promoting ENL mutation drives tumorigenesis *in vivo* through dynamic regulation of histone modifications and gene expression

Yiman Liu[1, 2, 15], Qinglan Li[1, 2, 15], Lele Song[1, 2], Chujie Gong[1, 2, 3], Sylvia Tang[1, 2], Krista A. Budinich[1, 2, 4], Ashley Vanderbeck[5, 6, 7], Kaeli M. Mathias[1, 2, 8, 9], Gerald B. Wertheim[10, 11], Son C. Nguyen[12, 13], Riley Outen[7], Eric F. Joyce[12, 13], Ivan Maillard[7], Liling Wan[1,2,12,14, #]

[1]Department of Cancer Biology, Perelman School of Medicine, University of Pennsylvania, Philadelphia, PA, 19104, USA

[2]Abramson Family Cancer Research Institute, Perelman School of Medicine, University of Pennsylvania, Philadelphia, PA, 19104, USA

[3]Cell and Molecular Biology Graduate Group, Perelman School of Medicine, University of Pennsylvania, Philadelphia, PA, 19104, USA

[4]Cancer Biology Graduate Group, Perelman School of Medicine, University of Pennsylvania, Philadelphia, PA, 19104, USA

[5]VMD-PhD program, School of Veterinary Medicine, University of Pennsylvania, PA 19104, USA

[6]Immunology Graduate Group, Perelman School of Medicine, University of Pennsylvania, Philadelphia, PA, 19104, USA

[7]Division of Hematology/Oncology, Department of Medicine, Perelman School of Medicine, University of Pennsylvania, Philadelphia, PA 19104, USA

[8]Biochemistry and Molecular Biophysics Graduate Group, Perelman School of Medicine, University of Pennsylvania, Philadelphia, PA, 19104, USA

[9]Center for Computational and Genomic Medicine, The Children's Hospital of Philadelphia, Philadelphia, PA 19104, USA

[10]Department of Pathology and Laboratory Medicine, Department of Medicine, Perelman School of Medicine, University of Pennsylvania, Philadelphia, PA 19104, USA

[11]Division of Hematopathology, The Children's Hospital of Philadelphia, Philadelphia, PA 19104, USA

[12]Epigenetics Institute, Perelman School of Medicine, University of Pennsylvania, Philadelphia, PA, 19104, USA.

[13]Department of Genetics, Perelman School of Medicine, University of Pennsylvania, Philadelphia, PA, 19104, USA

[14]Institute for Regenerative Medicine, Perelman School of Medicine, University of Pennsylvania, Philadelphia, PA, 19104, USA

[15]These authors contributed equally

[#]Corresponding Authors:
Liling Wan, University of Pennsylvania, BRB II/III, RM751, 421 Curie Blvd, Philadelphia, PA 19104.
Phone: 215-898-3116; E-mail: Liling.Wan@Pennmedicine.upenn.edu

Running title: Condensate-promoting ENL mutations as a driver of AML

Keywords: transcriptional condensates, acute myeloid leukemia, ENL mutations, histone acetylation, histone methylation, hematopoietic development, small-molecule inhibitor

Conflict of Interest: L.W. is a co-inventor on a patent filed (US No. 62/949,160) related to the inhibitor used in this manuscript and is a consultant for Bridge Medicines. I.M. has received research funding from Genentech and Regeneron and serves on the scientific advisory board of Garuda Therapeutics (all unrelated to the contents of this manuscript). Other authors declare that they have no competing financial interests.

Supplementary Figures with Legends

Supplementary Figure S16. ENL mutants form condensate at key target genes and increase gene expression in HSPCs.

Supplementary Figure S17. Condensate formation property correlates with mutant *ENL*'s oncogenic function in human $CD34^+$ HSPCs.

Supplementary Figure S18. Expression levels of different FLAG-*ENL* transgenes in LSK cells.

Supplementary Figure S19. Condensate formation property correlates with mutant ENL's oncogenic function in GMP cells.

Supplementary Figure S20. Disrupting condensate formation by the H116P mutation reduces ENL-T1-induced increases in chromatin occupancy of FLAG-*ENL*, H3K27ac, and p300 at a subset of target genes.

Supplementary Figure S21. Impact of mutant ENL on leukemia development and condensate formation.

Supplementary Figure S22. Small molecule inhibition of the acetyl-binding activity of mutant ENL suppresses chromatin function and *Hoxa* cluster gene activation in LSK cells.

Supplementary Figure S23. Small molecule inhibition of the acetyl-binding activity of mutant ENL impairs its chromatin and transcriptional function in HSPCs.

Supplementary Figure S24. Small molecule inhibition of the acetyl-binding activity of mutant ENL inhibits its impact on the self-renewal property in HSPCs.

Supplementary Tables

Supplementary Table S1. Genes differentially expressed between *Enl*-T1 and *Enl*-WT LSK cells.

Supplementary Table S2. Genes differentially expressed between *Enl*-T1 and *Enl*-WT GMP cells.

Supplementary Table S3. Genes differentially expressed between *Enl*-T1 and *Enl*-WT L-GMP cells.

Supplementary Table S4. Genes differentially expressed between *Enl*-T1 and *Enl*-WT $cKit^+Mac1^+$ cells.

Supplementary Table S5. Genes differentially expressed between *Enl*-T1 and *Enl*-WT $cKit^-Mac1^+$ cells.

Supplementary Table S6. Shared *Enl*-T1 up-regulated DEGs in LSK, GMP, and L-GMP cells.

Supplementary Table S7. Expression of Hoxa genes in *Enl*-WT and *Enl*-T1 hematopoietic populations.

Supplementary Table S8. GSEA gene sets used in Supplementary Figure S12.

Supplementary Table S9. GSVA score of patients from TARGET-AML database.

Supplementary Table S10. H3K27ac peaks in all hematopoietic populations.

Supplementary Table S11. H3K27ac differential regions of ENL-T1 versus ENL-WT in LSK cells.

Supplementary Table S12. H3K27ac differential regions of ENL-T1 versus ENL-WT in GMP cells.

Supplementary Table S13. H3K27ac differential regions of ENL-T1 versus ENL-WT in L-GMP cells.

Supplementary Table S14. H3K27ac differential regions of ENL-T1 versus ENL-WT in $cKit^{+}Mac1^{+}$ cells.

Supplementary Table S15. H3K27ac differential regions of ENL-T1 versus ENL-WT in $cKit^{-}Mac1^{+}$ cells.

Supplementary Table S16. T1-UP DEGs associated with H3K27ac T1 gained DRs in all hematopoietic populations.

Supplementary Table S17. H3K27ac T1 gained differential regions associated with T1-UP DEGs in all hematopoietic populations.

Supplementary Table S18. p300 ChIP-seq normalized signal at T1 gained H3K27ac differential regions in *Enl*-WT and *Enl*-T1 GMP, L-GMP cells.

Supplementary Table S19. T1 gained H3K27ac differential regions with both p300 UP and associated gene expression UP in *Enl*-T1 cells for GMP and L-GMP.

Supplementary Table S20. T1 gained H3K27ac differential regions with p300 UP and associated gene expression UP in *Enl*-T1 cells for L-GMP under A-485 treatment.

Supplementary Table S21. H3K27me3 peaks in wildtype hematopoietic populations.

Supplementary Table S22. Hematopoietic differentiation associated-H3K27me3 peaks.

Supplementary Table S23. H3K27me3 peaks in all hematopoietic populations.

Supplementary Table S24. H3K27me3 differential regions of ENL-T1 versus ENL-WT in LSK cells.

Supplementary Table S25. H3K27me3 differential regions of ENL-T1 versus ENL-WT in GMP cells.

Supplementary Table S26. H3K27me3 differential regions of ENL-T1 versus ENL-WT in L-GMP cells.

Supplementary Table S27. H3K27me3 differential regions of ENL-T1 versus ENL-WT in cKit^{+}Mac1^{+} cells.

Supplementary Table S28. H3K27me3 differential regions of ENL-T1 versus ENL-WT in cKit^{-}Mac1^{+} cells.

Supplementary Table S29. T1-UP DEGs associated with H3K27me3 lost differential regions in all hematopoietic populations.

Supplementary Table S30. Group1 and group2 gene list in cKit^{+}Mac1^{+} and cKit^{-}Mac1^{+} cells.

Supplementary Table S31. FLAG-ENL peaks in LSK cells expressing the indicated FLAG-ENL transgenes.

Supplementary Table S32. FLAG-ENL gained regions of T1 versus WT in LSK cells expressing the indicated FLAG-ENL transgenes.

Supplementary Table S33. H3K27ac T1 gained differential regions associated with T1 gained FLAG-ENL DRs in LSK cells expressing the indicated FLAG-ENL transgenes.

Supplementary Table S34. Genes differentially expressed between *Enl*-T1-DMSO and *Enl*-WT-DMSO LSK cells.

Supplementary Table S35. Genes differentially expressed between *Enl*-T1-DMSO and *Enl*-WT-DMSO in GMP cells.

Supplementary Table S36. Expression of Hoxa genes under *Enl*-WT-DMSO, *Enl*-T1-DMSO and *Enl*-T1-TDI conditions in LSK and GMP cells.

Supplementary Table S37. Oligos used in this study.

Supplementary Table S38. Antibodies used in this study.

Supplementary Figure S1

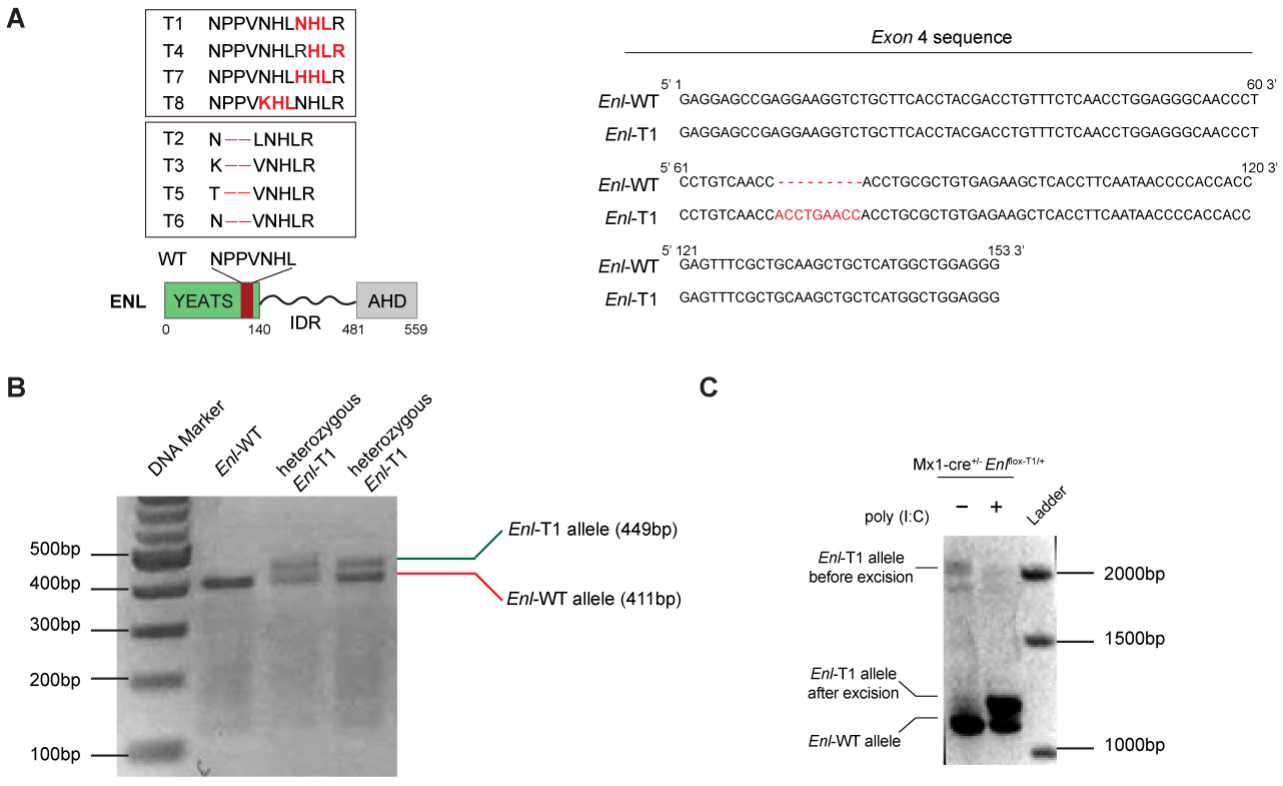

Supplementary Figure S1. Generation of a conditional knock-in mouse model for the *Enl*-T1 mutation. A, Left, the domain structure of the ENL protein and protein sequence differences for ENL WT and mutants (T1-T8). Right, the DNA sequence of WT or T1 mutation-containing exon 4 in the *Enl* gene. The insertion is highlighted in red. IDR, intrinsically disordered region; AHD, ANC1 homologue domain. **B,** Genotyping PCR showing DNA bands for *Enl*-WT and *Enl*-T1 alleles before Cre-mediated recombination. Primers F1/R1 shown in Figure 1A were used. **C,** PCR analysis showing the recombination efficiency of the *Enl*-T1 allele in *Enl*-T1 mice before and after poly (I:C) treatment. Primers F2/R2 shown in Figure 1A were used to identify the WT and T1 alleles in both before and after cre-mediated recombination conditions.

Supplementary Figure S2

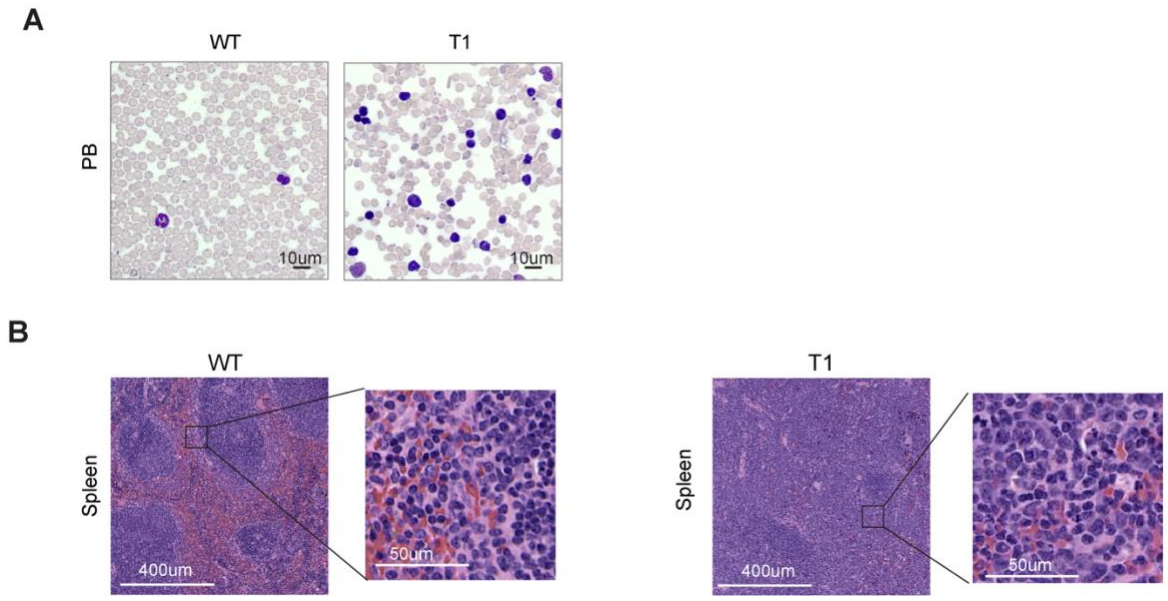

Supplementary Figure S2. Impact of *Enl* mutation on the peripheral blood and spleen. A, Wright–Giemsa-stained smear of PB harvested from *Enl*-T1 mice and age-matched control mice. PB, peripheral blood. Scale bar, 10 μm. **B,** Representative hematoxylin and eosin (H&E) staining of spleen harvested from *Enl*-WT or T1 mice. Scale bar, 400 μm (left, zoomed out); 50 μm (right, zoomed in).

196 **Supplementary Figure S3**

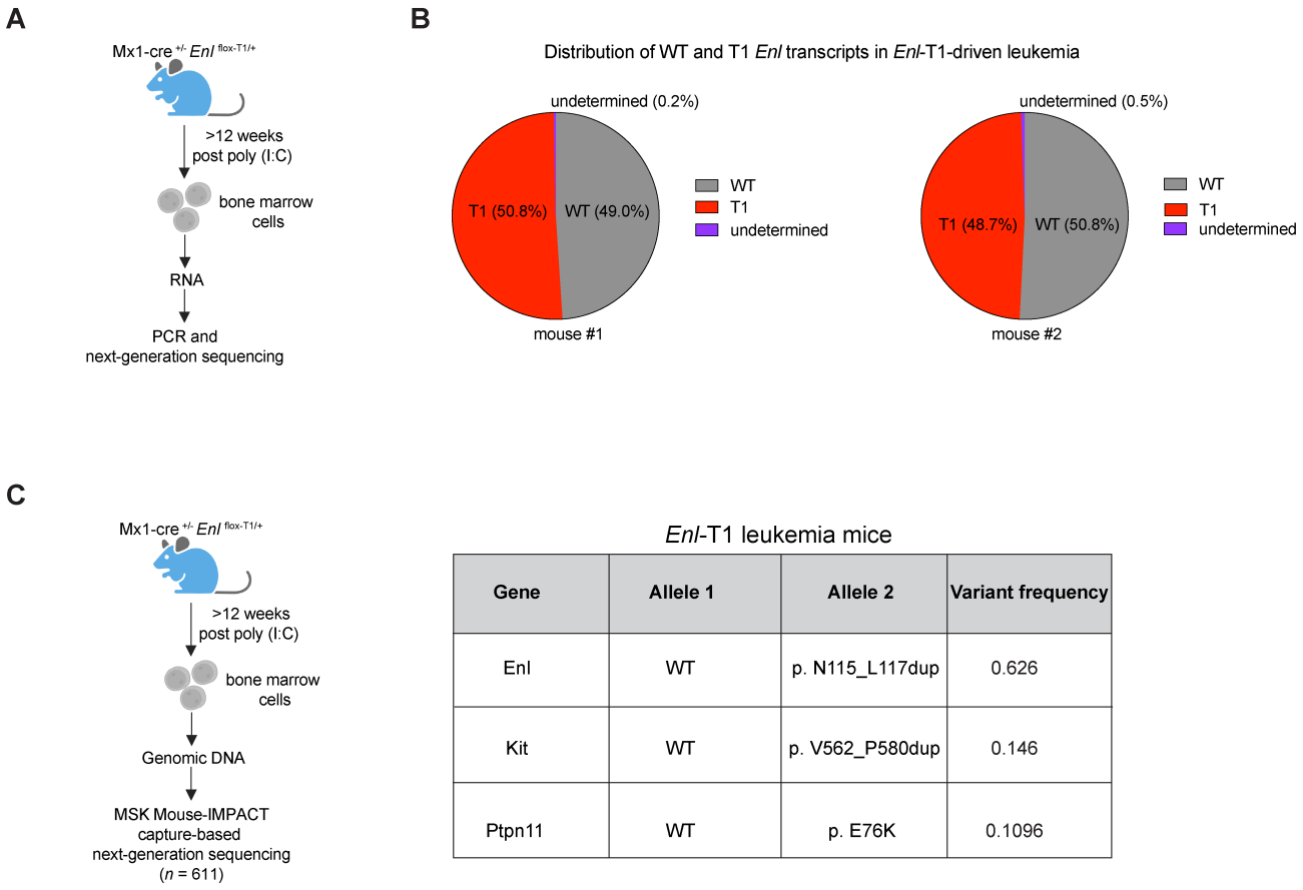

Enl-T1 leukemia mice

Gene	Allele 1	Allele 2	Variant frequency
Enl	WT	p. N115_L117dup	0.626
Kit	WT	p. V562_P580dup	0.146
Ptpn11	WT	p. E76K	0.1096

Supplementary Figure S3. Characterization of *Enl*-T1 allele expression and concurrent mutations in heterozygous knock-in *Enl*-T1 mouse model. A, Schematic workflow of *Enl*-WT and T1 transcripts analysis for *Enl*-T1 bone marrow cells. **B,** Pie charts showing the distribution of *Enl*-WT and T1 transcripts in *Enl*-T1-driven leukemia. *Enl*-WT allele (grey), *Enl*-T1 allele (red), undetermined allele (purple). **C,** Workflow (left) and detected mutations (right) in *Enl*-T1-driven leukemia.

197
198

Supplementary Figure S4

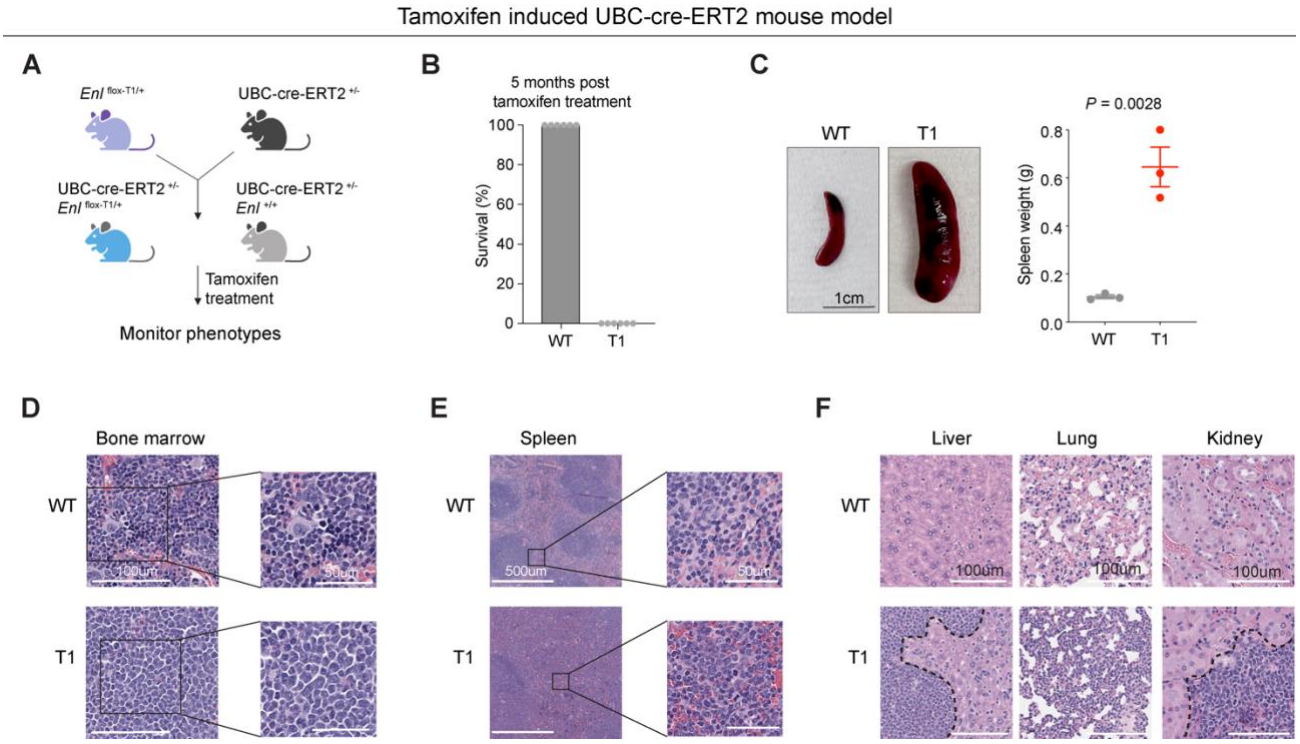

Supplementary Figure S4. UBC-cre-ERT2/*Enl* $^{flox\text{-}T1/+}$ mice develop aggressive acute leukemia following tamoxifen treatment. A, Breeding strategies to obtain UBC-cre-ERT2/*Enl* $^{flox\text{-}T1/+}$ mice for experiments. **B,** Quantification plot showing survival percentage of *Enl*-WT (n = 5) or *Enl*-T1 (n = 5) mice post tamoxifen treatment for 5 months. WT, UBC-cre-ERT2/*Enl* $^{+/+}$; T1, UBC-cre-ERT2/*Enl* $^{flox\text{-}T1/+}$. **C,** Representative images (left) and weight quantification (right) of spleen harvested from *Enl*-WT or T1 mice. Scale bar, 1 cm; Bars represent the median (n = 3). P value using unpaired, two-tailed Student's t-test. **D, E,** Representative hematoxylin and eosin (H&E) staining of bone marrow (**D**) and spleen (**E**) harvested from *Enl*-WT or T1 mice. Scale bar for bone marrow, 100 μm (left, zoomed out); 50 μm (right, zoomed in). Scale bar for spleen, 500 μm (left, zoomed out); 50 μm (right, zoomed in). **F,** Representative H&E staining of liver (left), lung (middle), kidney (right) harvested from *Enl*-WT or T1 mice. Scale bar, 100 μm.

Supplementary Figure S5

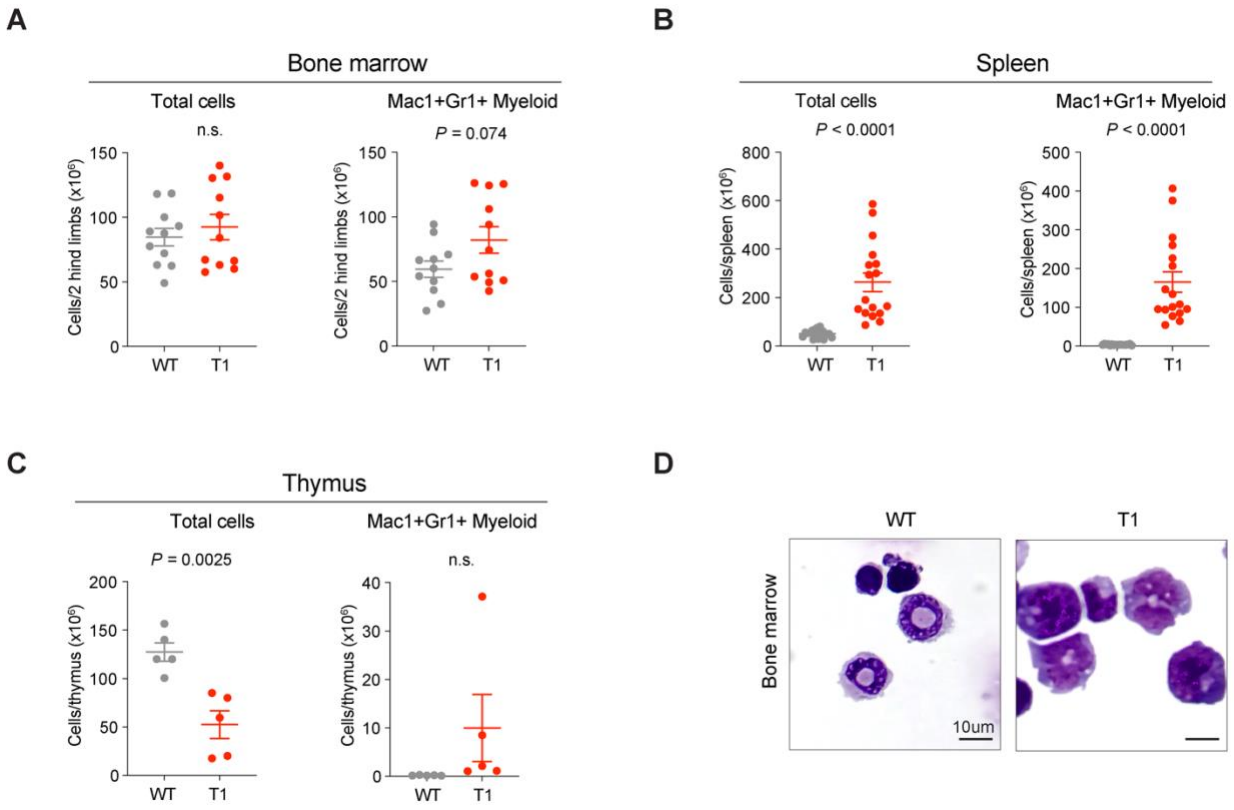

Supplementary Figure S5. *Enl* mutation leads to expansion of myeloid cells in mice in the leukemic phase. A-C, Number of total cells (left) and $Mac1^{+}Gr1^{+}$ myeloid cells (right) in bone marrow (**A**), spleen (**B**), and thymus (**C**) samples harvested from *Enl*-T1 leukemic mice and age-matched control mice. Bars represent the median (bone marrow, $n = 11$; spleen, $n = 17$; thymus, $n = 5$). *P* value using unpaired, two-tailed Student's *t*-test. n.s., not significant. **D,** Wright–Giemsa-stained smear of bone marrow harvested from *Enl*-T1 leukemic mice and age-matched control mice. Scale bar, 10 μm.

Supplementary Figure S6

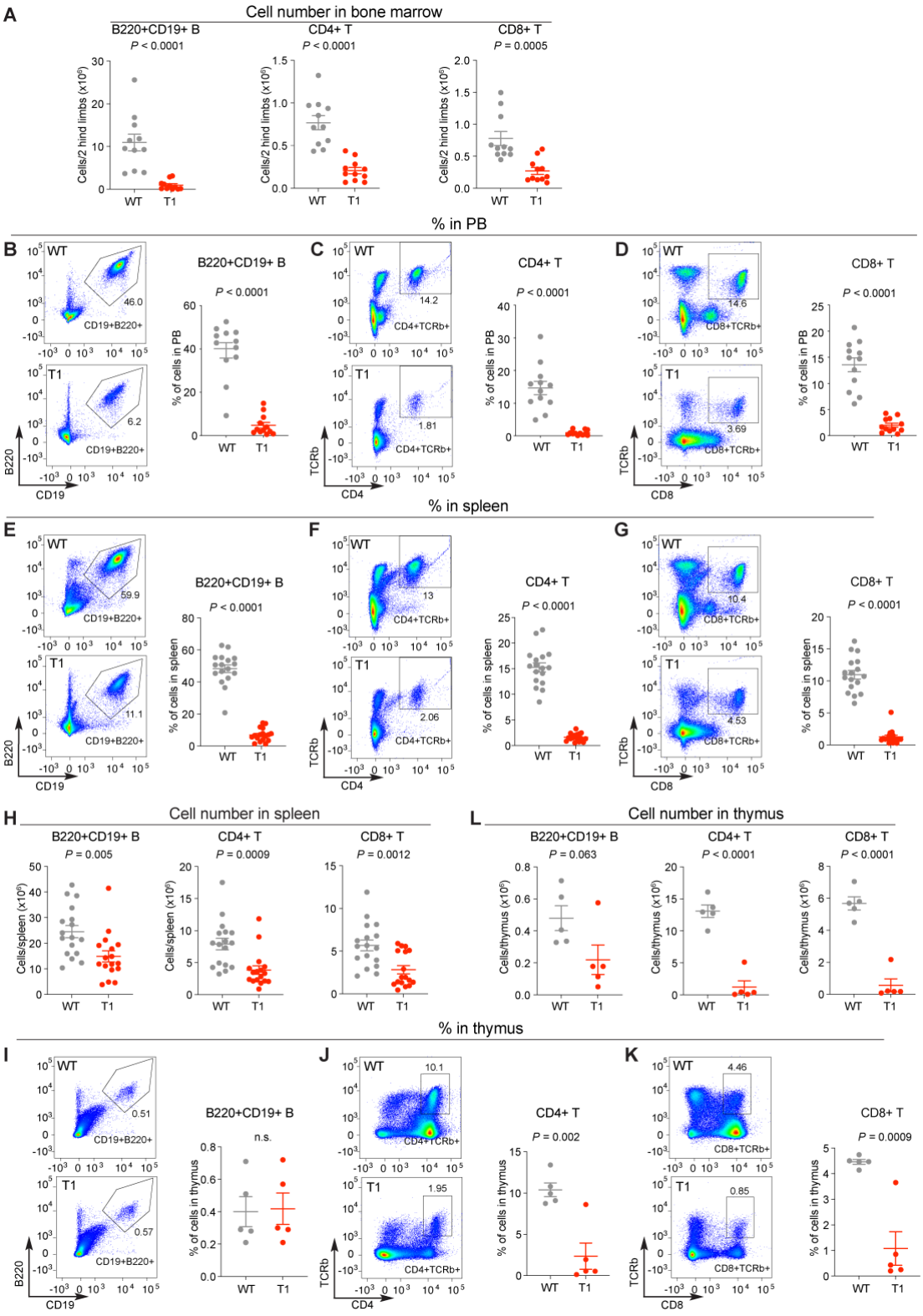

Supplementary Figure S6. *Enl* mutation leads to the decrease of B220$^+$CD19$^+$ B, CD4$^+$T, CD8$^+$ T cells in mice in the leukemic phase. A, Number of B220$^+$CD19$^+$ B (left), CD4$^+$T (middle), CD8$^+$ T (right) cells in bone marrow samples harvested from *Enl*-T1 leukemic mice and age-matched control mice. n = 11. **B-D,** Representative flow cytometric plots and percentage of B220$^+$CD19$^+$ B (**B**), CD4$^+$T (**C**), CD8$^+$ T (**D**) cells in PB samples harvested from *Enl*-T1 leukemic mice and age-matched control mice. n = 12. **E-G,** Representative flow cytometric plots and the percentage of B220$^+$CD19$^+$ B (**E**), CD4$^+$T (**F**), CD8$^+$ T (**G**) cells in spleen samples harvested from *Enl*-T1 leukemic mice and age-matched control mice. n = 17. **H,** Number of B220$^+$CD19$^+$ B (left), CD4$^+$T (middle), CD8$^+$ T (right) cells in spleen samples harvested from *Enl*-T1 leukemic mice and age-matched control mice. n = 17. **I-K,** Representative flow cytometric plots and the percentage of B220$^+$CD19$^+$ B (**I**), CD4$^+$T (**J**), CD8$^+$ T (**K**) cells in thymus samples harvested from *Enl*-T1 leukemic mice and age-matched control mice. n = 5. **L,** Number of B220$^+$CD19$^+$ B (left), CD4$^+$T (middle), CD8$^+$ T (right) cells in thymus samples harvested from *Enl*-T1 leukemic mice and age-matched control mice. n = 5. **A-L,** Bars represent the median; P value using unpaired, two-tailed Student's t-test. n.s., not significant.

206

Supplementary Figure S7

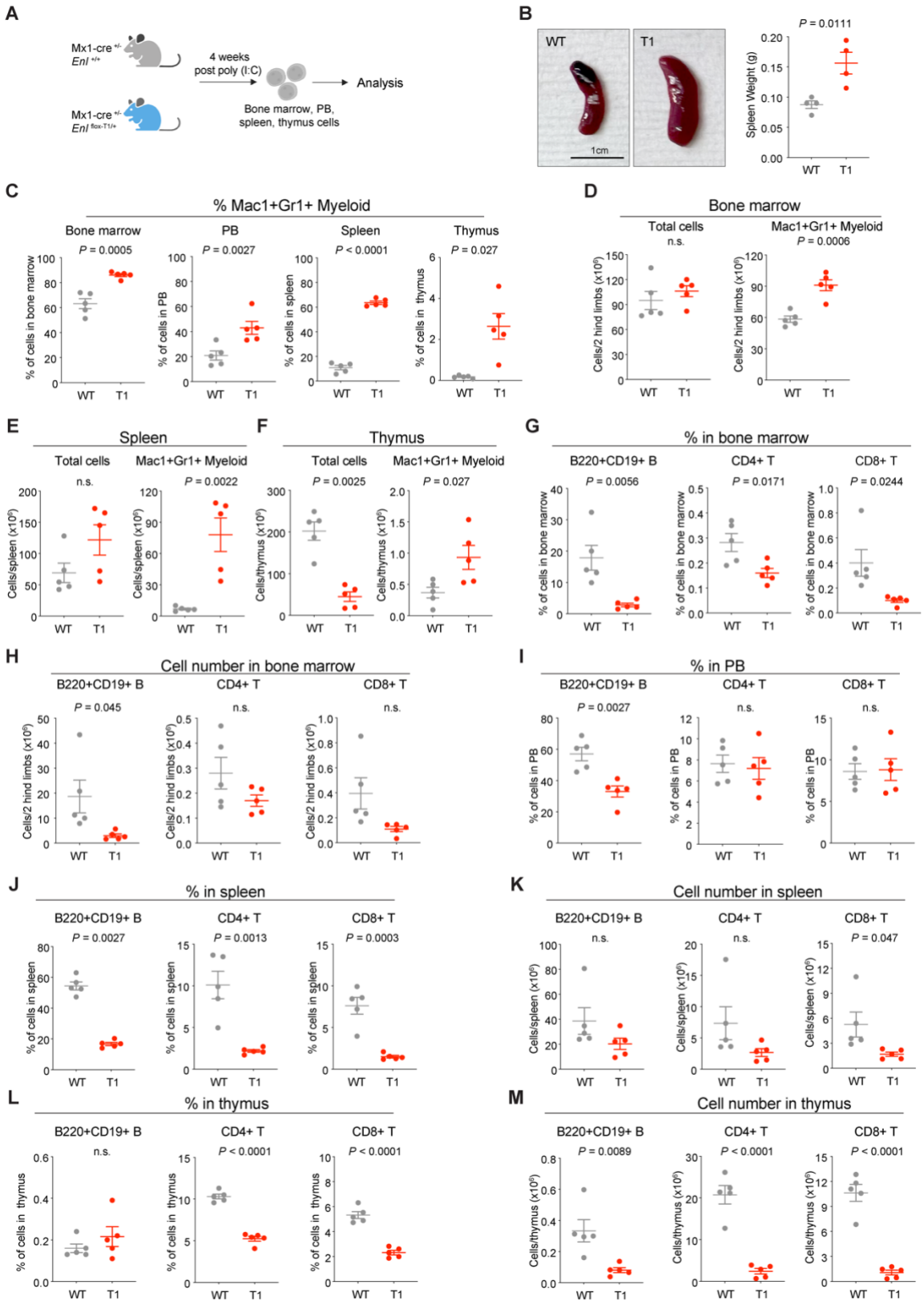

209

Supplementary Figure S7. Impact of the *Enl* mutation on the bone marrow, peripheral blood, spleen, and thymus in mice in the pre-leukemic phase. A, Schematic of experimental workflow of *Enl*-T1 pre-leukemic mice and age-matched control mice (shown in **B-M**). **B,** Representative images (left) and weight quantification (right) of spleen. Scale bar, 1 cm; $n = 4$. **C,** Percentage of $Mac1^+Gr1^+$ myeloid cell population in the bone marrow (left), PB (center left), spleen (center right), and thymus (right) samples. $n = 5$. **D-F,** Number of total cells (left) and $Mac1^+Gr1^+$ myeloid cells (right) in bone marrow (**D**), spleen (**E**), and thymus (**F**) samples. $n = 5$. **G, H,** Percentage (**G**) and number (**H**) of $B220^+CD19^+$ B (left), $CD4^+$T (middle), $CD8^+$ T (right) cells in bone marrow samples. $n = 5$. **I,** Percentage of $B220^+CD19^+$ B (left), $CD4^+$T (middle), $CD8^+$ T (right) cells in peripheral blood samples. $n = 5$. **J, K,** Percentage (**J**) and number (**K**) of $B220^+CD19^+$ B (left), $CD4^+$T (middle), $CD8^+$ T (right) cells in spleen samples. $n = 5$. **L, M,** Percentage (**L**) and number (**M**) of $B220^+CD19^+$ B (left), $CD4^+$T (middle), $CD8^+$ T (right) cells in thymus samples. $n = 5$. **B-M,** Bars represent the median; *P* value using unpaired, two-tailed Student's *t*-test. n.s., not significant.

210

Supplementary Figure S8

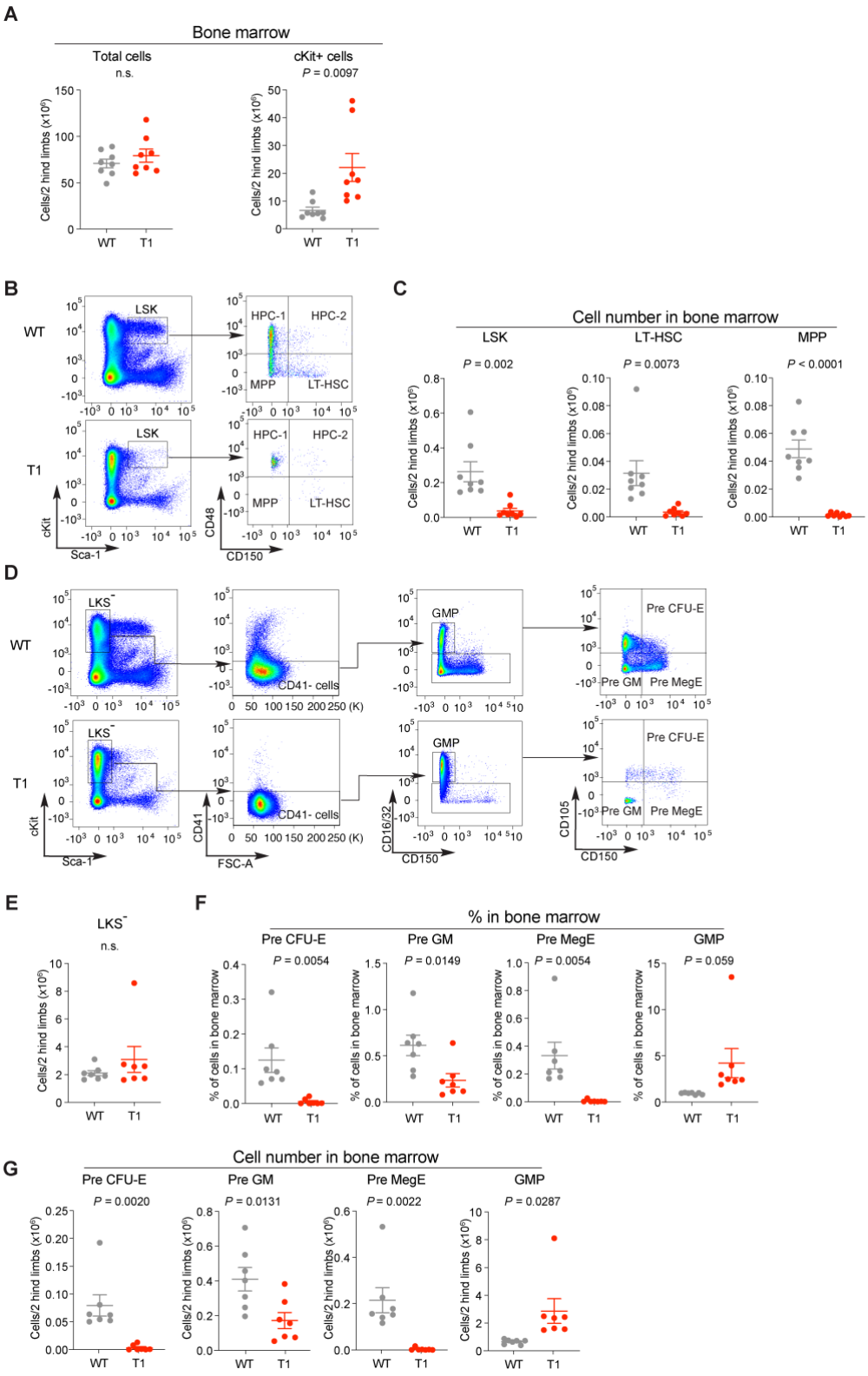

Supplementary Figure S8. *Enl* mutation perturbs the normal hematopoietic hierarchy and leads to abnormal expansion of myeloid progenitors in mice in the leukemic phase. A, Number of total cells (left) and cKit$^+$ cells (right) in bone marrow samples (see workflow in **Fig.2B**). *n* = 8. **B, C,** Representative flow cytometric plots (**B**) and number (**C**) of LSK, LT-HSC, and MPP cells in bone marrow (see workflow in **Fig.2B**). *n* = 8. **D,** Representative flow cytometric plots of LKS$^-$, GMP, Pre CFU-E, Pre GM, and Pre MegE cells in bone marrow samples (see workflow in **Fig.2B**). **E,** Number of LKS$^-$ cells in bone marrow samples (see workflow in **Fig.2B**). *n* = 7. **F, G,** Percentage (**F**) and number (**G**) of Pre CFU-E (left), Pre GM (center left), Pre MegE (center right), and GMP (right) cells in bone marrow (see workflow in **Fig.2B**). *n* = 7. **A, C, E-G,** Bars represent the median; *P* value using unpaired, two-tailed Student's *t*-test. n.s., not significant.

213

214 **Supplementary Figure S9**

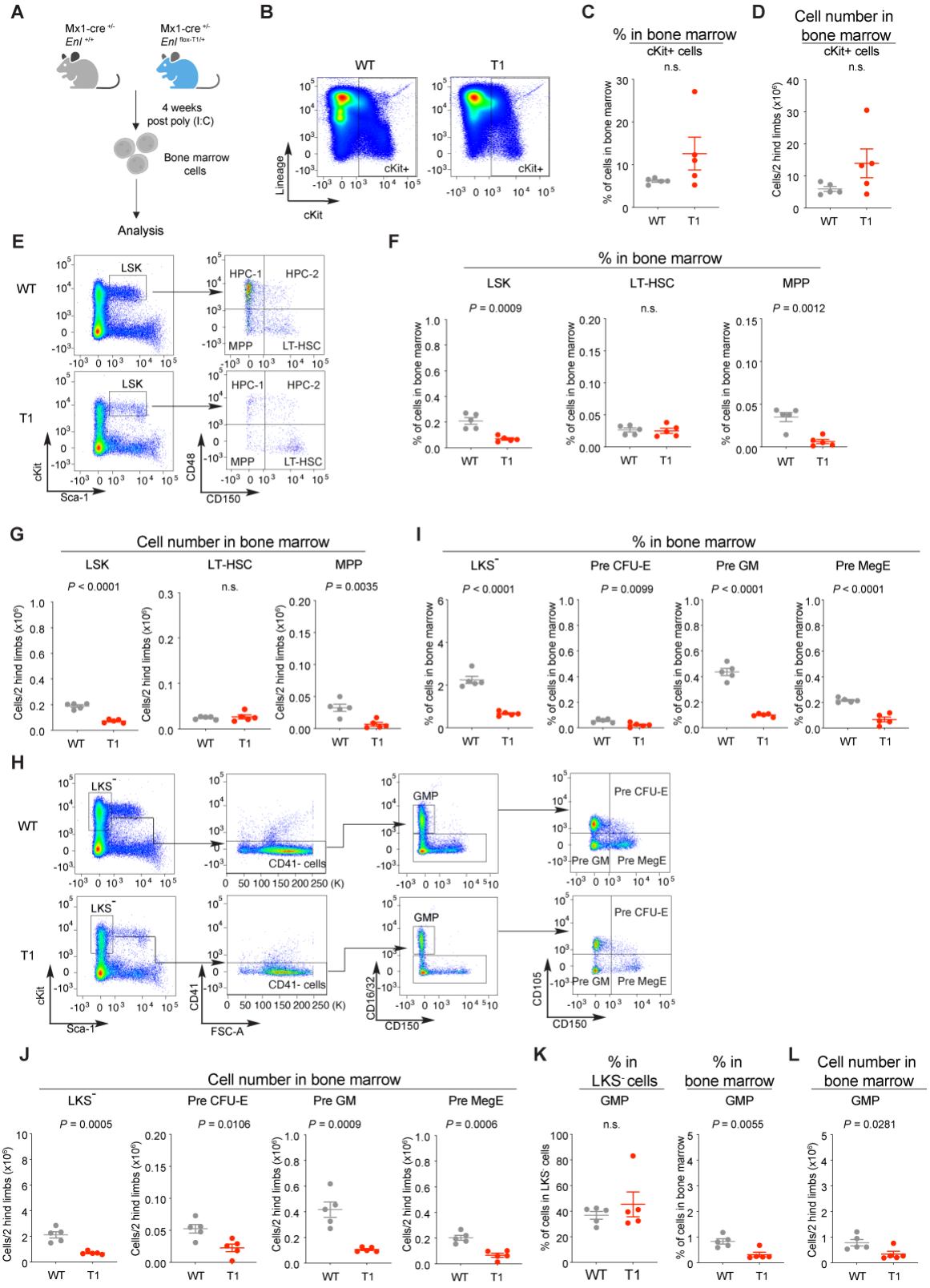

Supplementary Figure S9. *Enl* mutation does not lead to the expansion of myeloid progenitors in mice in the pre-leukemic phase. A, Schematic workflow of flow cytometric analysis for bone marrow cells from *Enl*-T1 pre-leukemic mice and age-matched control mice (shown in **B-K**). **B-D,** Representative flow cytometric plots (**B**), percentage (**C**), and number (**D**) of $cKit^+$ cells in bone marrow samples. *n* = 5. **E-G,** Representative flow cytometric plots (**E**), percentage (**F**), and number (**G**) of LSK (left), LT-HSC (middle), and MPP (right) cells in bone marrow samples. *n* = 5. **H,** Representative flow cytometric plots of LKS^-, GMP, Pre CFU-E, Pre GM, and Pre MegE cells in bone marrow samples. **I, J,** Percentage (**I**) and number (**J**) of LKS^- (left), Pre CFU-E (center left), Pre GM (center right), Pre MegE (right) cells in bone marrow samples. *n* = 5. **K,** Percentage of GMP cells in LKS^- population (left) or bone marrow (right) samples. *n* = 5. **L,** Number of GMP cells in bone marrow samples. *n* = 5. **C, D, F, G, I-L,** Bars represent the median; *P* value using unpaired, two-tailed Student's *t*-test. n.s., not significant.

215

Supplementary Figure S10

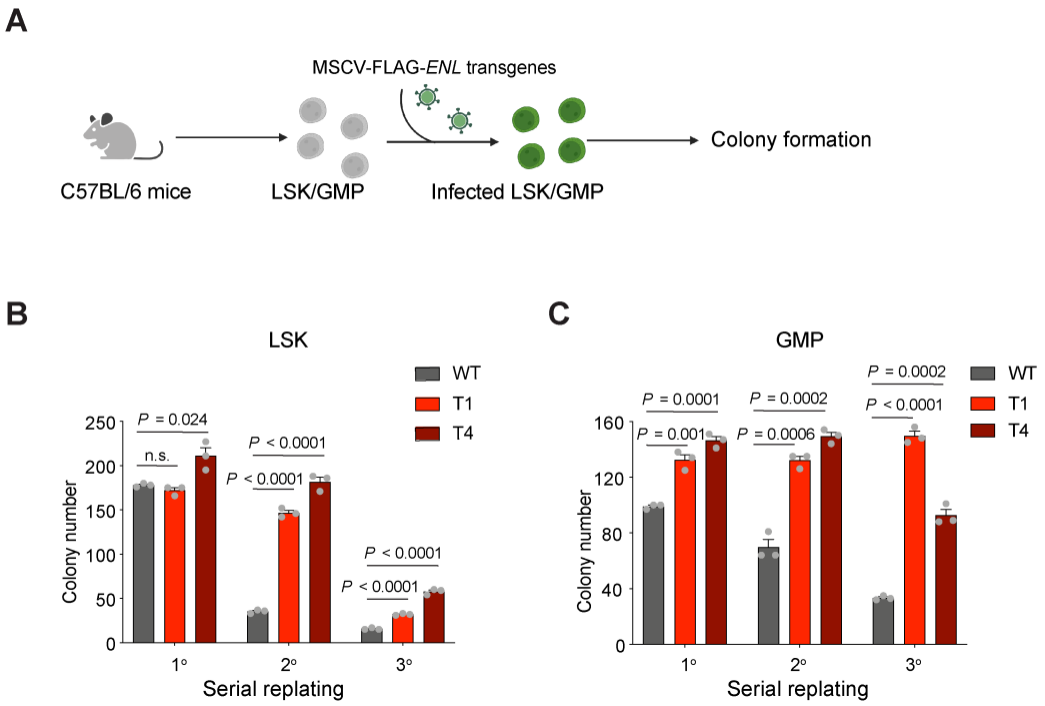

Supplementary Figure S10. *Enl* mutation promotes self-renewal properties of HSPCs. A, Schematic depiction of transduction of FLAG-GFP-tagged-*ENL* transgenes in LSK/GMP cells and subsequent colony formation assays. **B, C,** Quantification of colonies formed by LSK (**B**), GMP (**C**) cells expressing different FLAG-*ENL* transgenes. Error bars represent mean ± SEM (n = 3). P values using unpaired, two-tailed Student's t-test. n.s., not significant.

Supplementary Figure S11

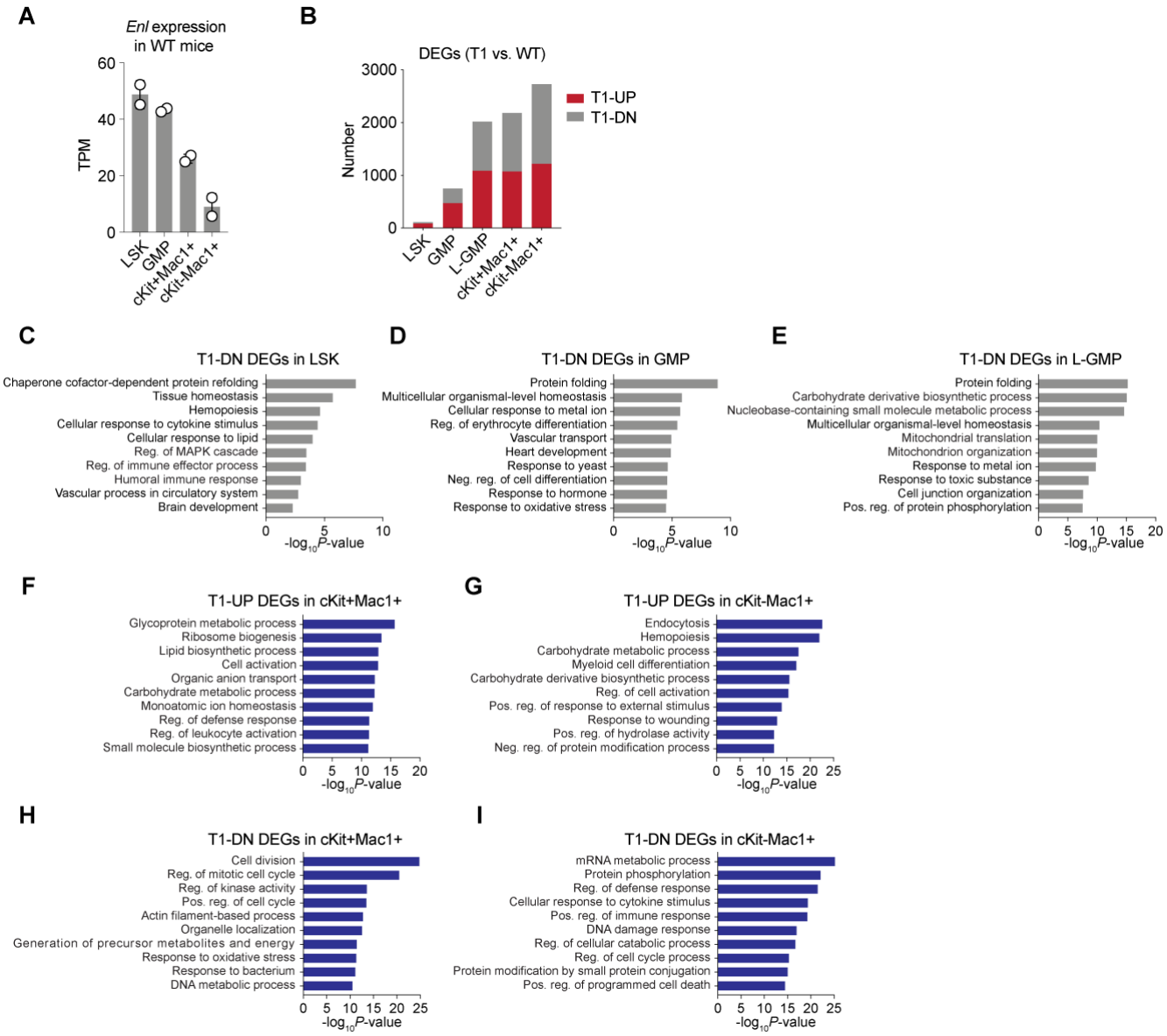

Supplementary Figure S11. *Enl* mutation-induced up- and down-regulated genes are related to distinct biological functions. A, Bar plots showing *Enl* expression in wild-type, normal hematopoietic populations. Gene expression is obtained from the RNA-seq data (see **Fig. 3A**) and normalized by transcripts per million (TPM). Dots represent different biological replicates. **B,** Stacked bar plots showing the number of *Enl*-T1-up and down-regulated genes in indicated cell populations. T1-UP, *Enl*-T1 up-regulated; T1-DN, *Enl*-T1 down-regulated; DEGs, differentially expressed genes. See Supplementary Tables S1-S5. **C-E,** Bar plots showing the GO-term analysis of T1-DN DEGs for LSK (**C**), GMP (**D**), L-GMP (**E**) cells. **F, G,** Bar plots showing the GO-term analysis of T1-UP DEGs for $cKit^{+}Mac1^{+}$ (**F**) and $cKit^{-}Mac1^{+}$ (**G**) cells. **H, I,** Bar plots showing the GO-term analysis of T1-DN DEGs for $cKit^{+}Mac1^{+}$ (**H**) and $cKit^{-}Mac1^{+}$ (**I**) cells. Pos., positive; Neg., negative; Reg., regulation.

220

Supplementary Figure S12

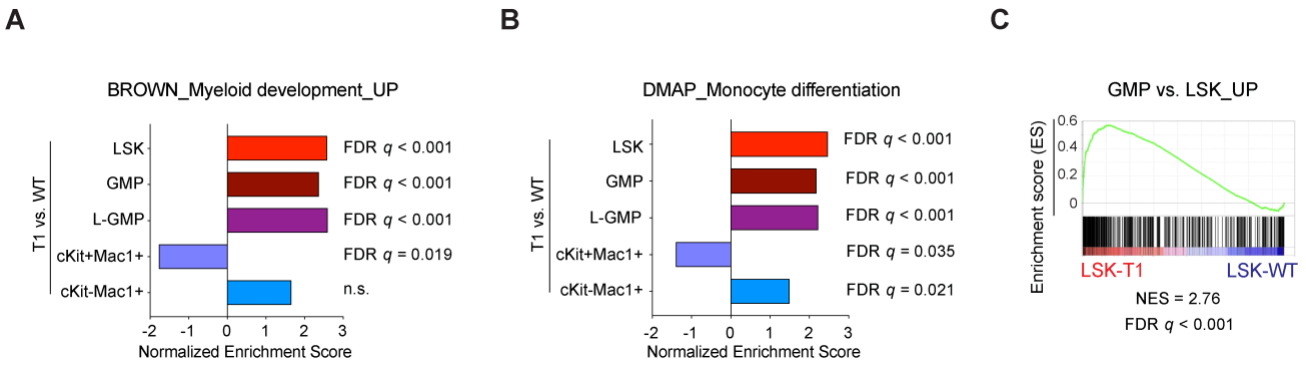

Supplementary Figure S12. *Enl* mutation leads to a gain of myeloid differentiation signatures in HSPCs. A, B, Normalized enrichment scores of Myeloid development_UP **(A)** and Monocyte differentiation (**B**) gene sets derived from GSEA analysis in indicated T1 cell populations when compared with WT counterparts. See Supplementary Table S8. **C,** GSEA plots evaluating gene expression changes in *Enl*-T1 versus *Enl*-WT LSK cells with genes upregulated in GMP versus LSK. FDR, false discovery rate; NES, normalized enrichment score. See Supplementary Table S8.

Supplementary Figure S13

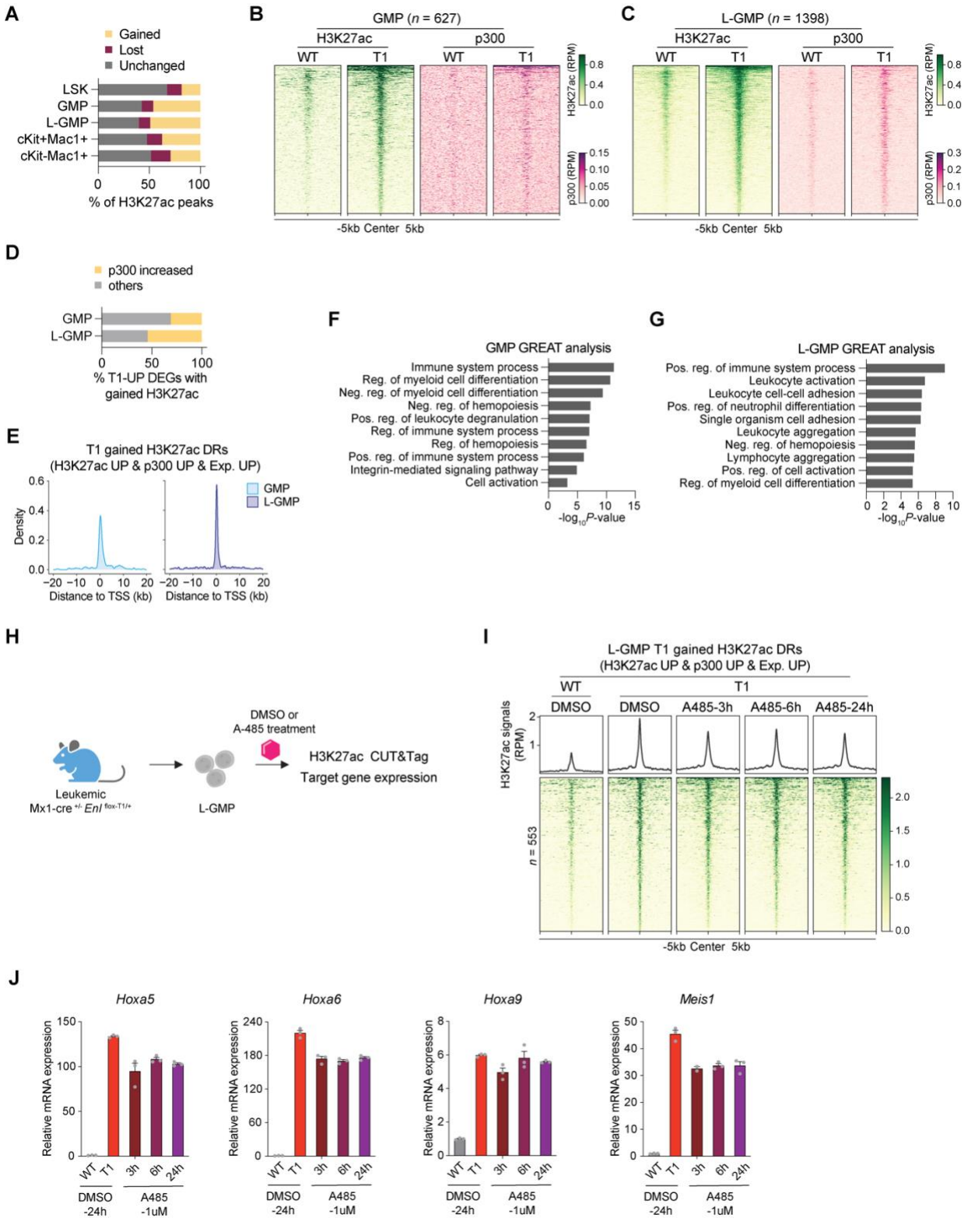

Supplementary Figure S13. Mutant ENL-induced H3K27ac signals correlate with upregulation of development and inflammation associated transcriptional programs. A, Stacked bar plots showing the percentage of T1 gained (yellow), lost (purple) and unchanged (grey) H3K27ac DRs in indicated cell populations. See Supplementary Tables S11-S15. **B, C,** Heatmap showing H3K27ac and p300 signals on T1-UP DEGs associated with gained H3K27ac DRs in GMP (**B**) and L-GMP (**C**) from *Enl*-WT or T1 mice. The CUT&Tag or ChIP-seq signals are normalized by RPM. See Supplementary Table S17. **D,** Stacked bar plots indicating the percentage of T1-UP DEGs with gained H3K27ac that also exhibited increased p300 occupancy (fold-change > 1.5). See Supplementary Table S18. **E,** Histogram showing that regions with an increase in p300 occupancy and H3K27ac signals and associated with T1-UP DEGs are located close to the TSS in GMP (left) and L-GMP (right). Exp., expression. See Supplementary Table S19. **F** and **G,** GREAT analysis of regions with an increase in p300 occupancy and H3K27ac signals and associated with T1-UP DEGs (identified in (D)) in GMP (**F**) and L-GMP (**G**). Pos., positive; Neg., negative; Reg., regulation. **H,** Schematic showing *ex vivo* treatment of L-GMP cells from *Enl*-T1 mice and subsequent experiments (shown in **I, J**). **I,** Average occupancies (top) and heatmap (bottom) of H3K27ac at genomic regions that exhibit T1-induced increases in H3K27ac and p300 and are associated with T1-UP DEGs in GMP (WT) or L-GMP (T1) cells treated with DMSO or A-485 (1 μM) for 24 hours. The CUT&Tag signals are normalized by RPM. See Supplementary Table S20. **J,** RT-qPCR analysis showing mRNA expression of *Hoxa5/6/9, Meis1* in GMP (WT) or L-GMP (T1) cells under indicated treatment conditions. Error bars represent mean ± SEM (n = 3).

Supplementary Figure S14

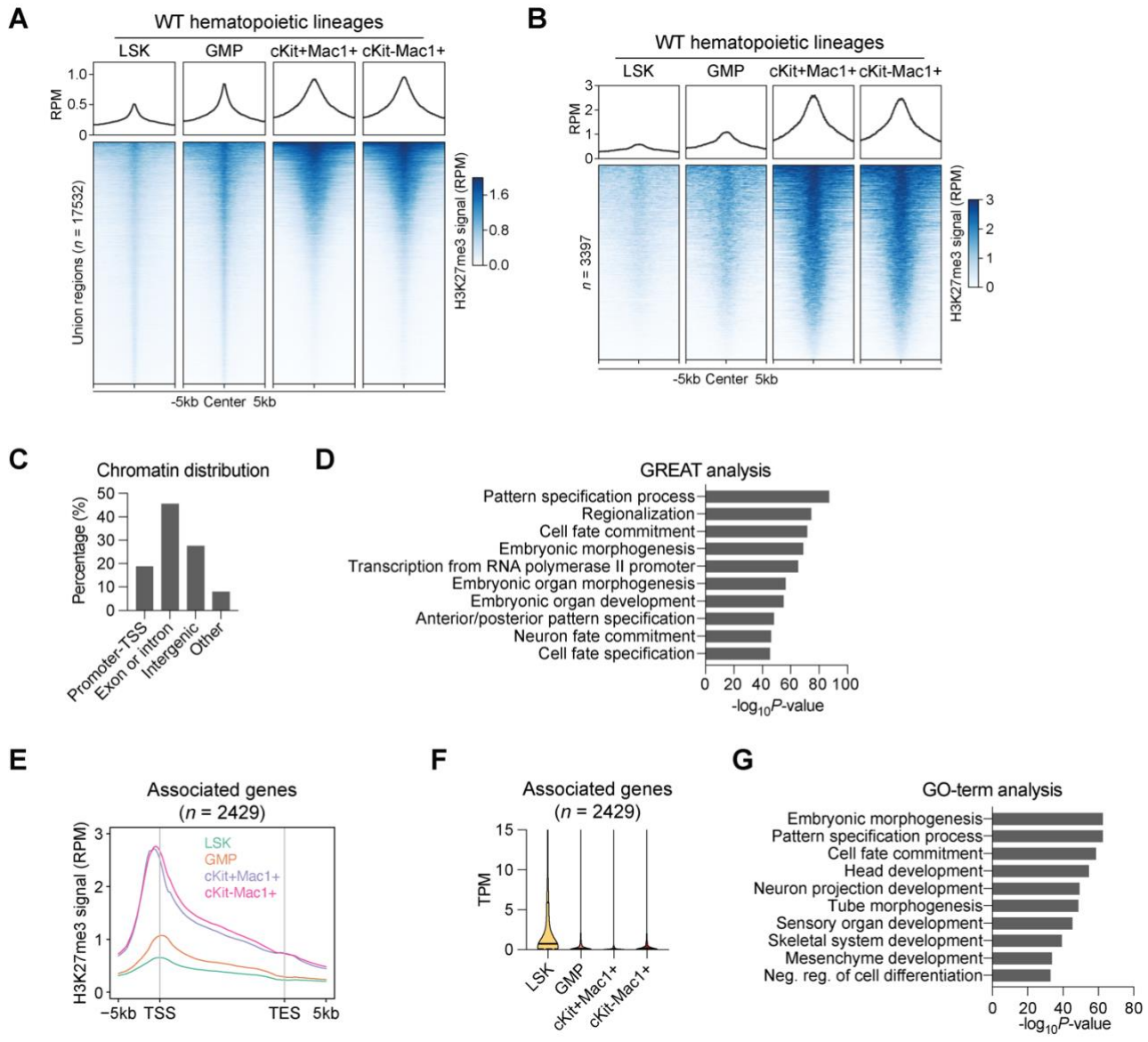

Supplementary Figure S14. HSPCs gain H3K27me3 during differentiation in wildtype mice. A, Average occupancies (top) and heatmap (bottom) of H3K27me3 signals showing dynamic changes of H3K27me3 during normal myeloid differentiation in wild-type mice. The union H3K27me3 peaks of normal LSK, GMP, $cKit^{+}Mac1^{+}$ and $cKit^{-}Mac1^{+}$ cells are used in both plots. See Supplementary Table S21. **B,** Average occupancies (top) and heatmap (bottom) of hematopoietic differentiation associated-H3K27me3 signals in LSK, GMP, $cKit^{+}Mac1^{+}$, and $cKit^{-}Mac1^{+}$ cells are defined by the following strategy. Among the union H3K27me3 peaks in (**A**), those exhibiting higher H3K27me3 signal in GMP compared with LSK cells, as well as higher H3K27me3 signal in $cKit^{+}Mac1^{+}$ and $cKit^{-}Mac1^{+}$ cells compared with GMP cells (fold-change > 1.5), were selected. These peaks were further filtered by their expression in both $cKit^{+}Mac1^{+}$ and $cKit^{-}Mac1^{+}$ subsets (RPM>1). See Supplementary Table S22. **C,** Bar plots showing the chromatin distribution of H3K27me3 DRs identified in (**B**). **D,** Bar plots showing the GREAT analysis of H3K27me3 DRs (identified in (**B**)). **E,** Average occupancies of H3K27me3 at H3K27me3 DRs (identified in (**B**)) associated genes in LSK, GMP, $cKit^{+}Mac1^{+}$ and $cKit^{-}Mac1^{+}$ cells. *n* = 2429; TSS, transcription start site; TES, transcription end site. **F,** Violin plots showing the gene expression of H3K27me3 DRs (identified in (**B**)) associated genes in LSK, GMP, $cKit^{+}Mac1^{+}$ and $cKit^{-}Mac1^{+}$ cells. Gene expression is obtained from the RNA-seq data and normalized by transcripts per million (TPM). **G,** Bar plots showing the GO-term analysis of H3K27me3 DRs (identified in (**B**)) associated genes.

Supplementary Figure S15

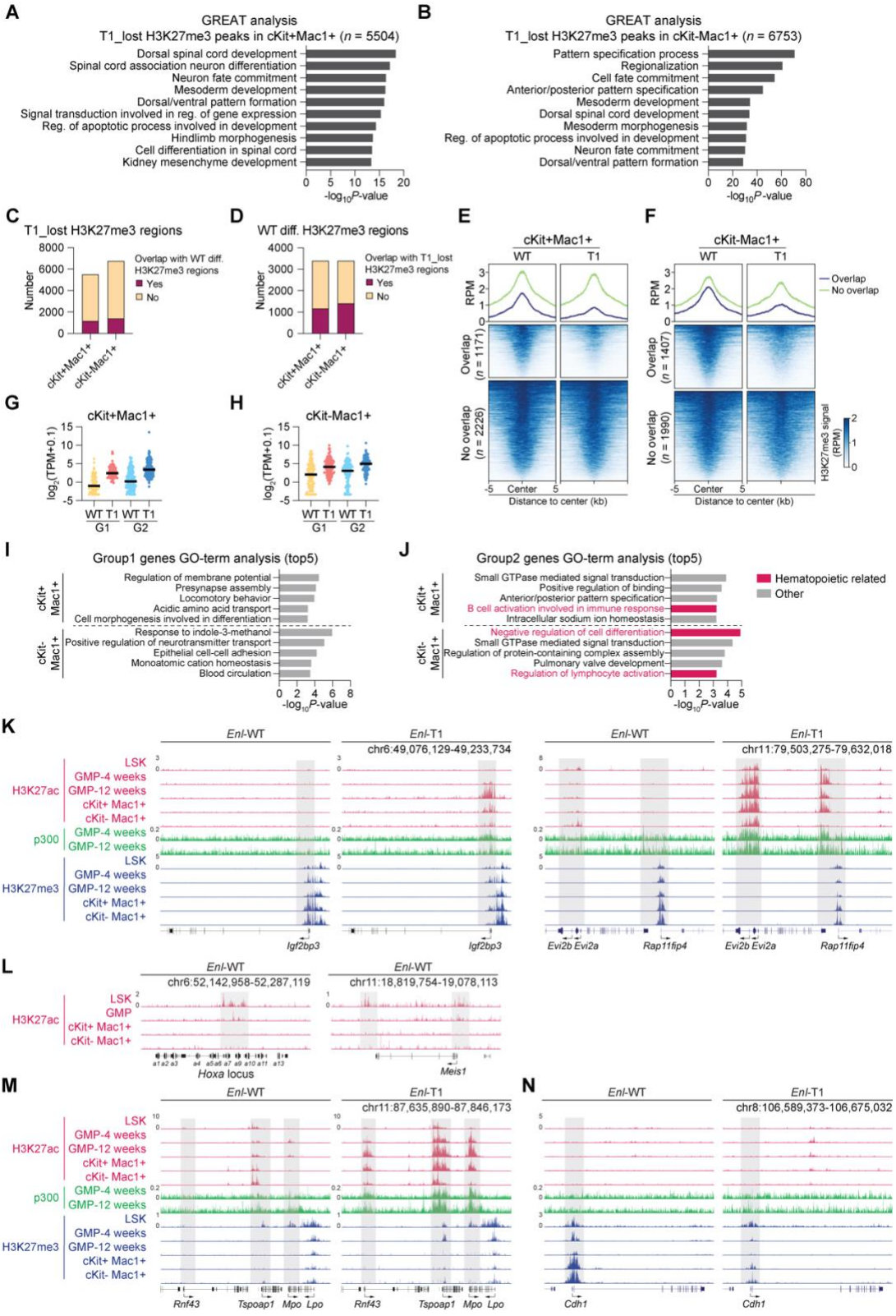

Supplementary Figure S15. Differentiation-associated gain of H3K27me3 is impaired in *Enl*-mutated hematopoietic cells. A, B, GREAT analysis of T1-lost H3K27me3 DRs in cKit$^+$Mac1$^+$ (**A**) and cKit$^-$Mac1$^+$ (**B**) cells. See Supplementary Tables S27 and S28. **C,** Stacked bar plots showing the numbers of T1-lost H3K27me3 DRs in cKit$^+$Mac1$^+$ and cKit$^-$Mac1$^+$ cells that are overlapped (purple) or not overlapped (yellow) with differentiation-associated H3K27me3 DRs (identified in **Supplemental Fig. 14B**). **D,** Stacked bar plots showing the numbers of differentiation associated H3K27me3 DRs (identified in **Supplemental Fig. 14B**) that are overlapped (purple) or not overlapped (yellow) with T1-lost H3K27me3 DRs in cKit$^+$Mac1$^+$ and cKit$^-$Mac1$^+$ cells. **E, F,** Average occupancies (top) and heatmap (bottom) of differentiation associated-H3K27me3 DRs (identified in **Supplemental Fig. 14B**) overlapped or not overlapped with T1 lost H3K27ac DRs in cKit$^+$Mac1$^+$ (**E**) and cKit$^-$Mac1$^+$ (**F**) cells. See Supplementary Table S22. **G, H,** Dot plots evaluating the expression difference between group1 and group2 genes in *Enl*-WT or T1 cKit$^+$Mac1$^+$ (**G**), cKit$^-$Mac1$^+$ (**H**) cells. The mean value is highlighted by the black bar in each group. Expression is normalized by $\log_2$(TPM+0.1). See Supplementary Table S30. **I**, **J,** Bar plots showing the GO-term analysis of group1 (**I**) and group2 (**J**) genes in cKit$^+$Mac1$^+$ (top) and cKit$^-$Mac1$^+$ (bottom). Hematopoietic related pathways are highlighted by red. **K,** The genome browser view of H3K27ac, p300 and H3K27me3 CUT&Tag or ChIP-seq signals at genes exhibiting T1-induced changes in both H3K27ac and H3K27me3 in indicated *Enl*-WT or T1 hematopoietic populations. **L,** The genome browser view of H3K27ac CUT&Tag signals at *Hoxa* (left) and *Meis1* (right) gene locus in *Enl*-WT hematopoietic populations with low signal scale. **M, N,** The genome browser view of H3K27ac, p300 and H3K27me3 CUT&Tag or ChIP-seq signals at genes exhibiting T1-induced changes in H3K27ac (**M**) or T1-induced changes in H3K27me3 (**N**) in indicated *Enl*-WT or T1 hematopoietic populations.

Supplementary Figure S16

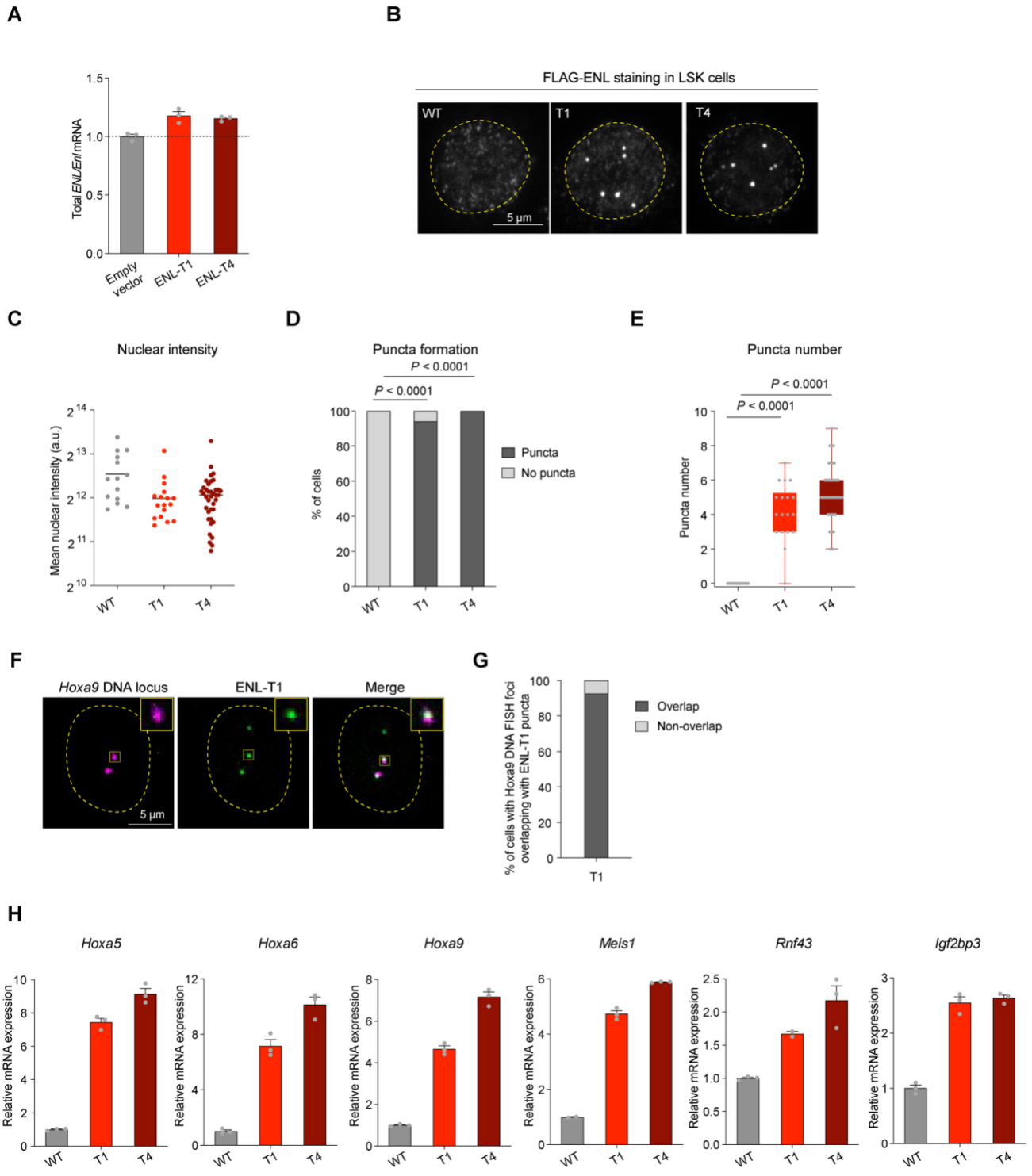

Supplementary Figure S16. ENL mutants form condensate at key target genes and increase gene expression in HSPCs. A, RT-qPCR analysis showing total mRNA levels of human and mouse *ENL/Enl* in LSK cells expressing empty vector or indicated human FLAG-*ENL* transgenes. The primers used for RT-qPCR can detect both human and mouse *ENL/Enl*. Error bars represent mean ± SEM (n = 3). **B,** Representative images of anti-FLAG IF staining in LSK cells expressing indicated FLAG-*ENL* transgenes. **C-E,** Nuclear intensity (**C**), percentage of nuclei with or without FLAG-ENL puncta (**D**), and the number of FLAG-ENL puncta (**E**) in each nucleus in LSK cells. Error bars represent mean ± SEM. *P* values using unpaired, two-tailed Student's *t*-test. **F, G,** Representative images (**F**) and quantification (**G**) showing percentage of LSK cells expressing FLAG-*ENL*-T1 transgene at least one *Hoxa9* DNA locus overlapping with an ENL-T1 puncta. n = 67. *P* value using unpaired, two-tailed Student's *t*-test. **H,** RT-qPCR analysis showing mRNA expression of *Hoxa5/6/9*, *Meis1*, *Rnf43*, *Igf2bp3* in LSK cells expressing indicated FLAG-*ENL* transgenes. Error bars represent mean ± SEM (n = 3).

238

Supplementary Figure S17

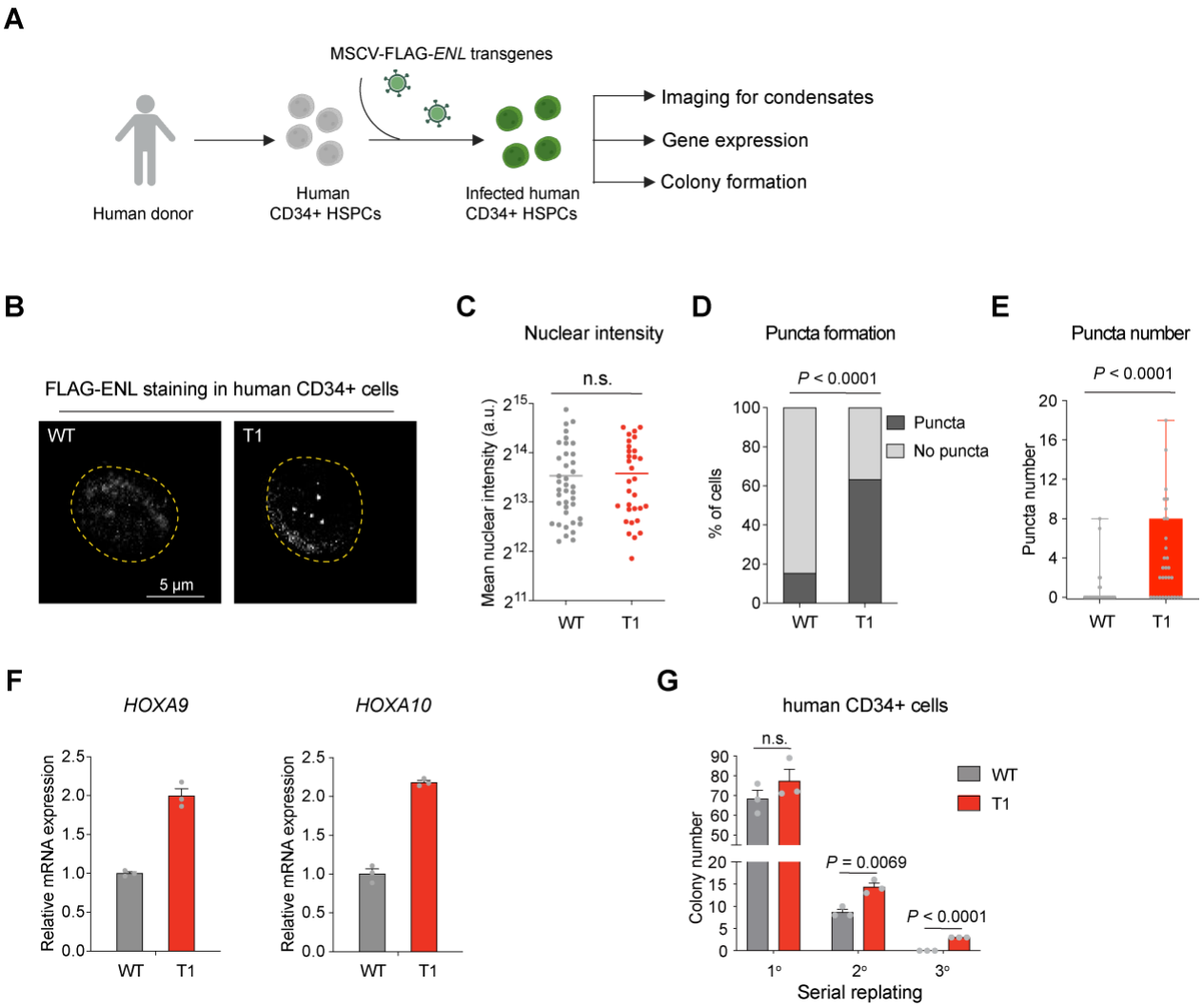

Supplementary Figure S17. Condensate formation property correlates with mutant *ENL*'s oncogenic function in human CD34$^+$ HSPCs. A, Schematic representation of the transduction of various FLAG-tagged *ENL* transgenes in human CD34$^+$ HSPCs and subsequent experiments (shown in **B-G**). **B,** Representative images of anti-FLAG IF staining in human CD34$^+$ HSPCs expressing indicated FLAG-*ENL* transgenes. **C-E,** Nuclear intensity (**C**), percentage of nuclei with or without FLAG-ENL puncta (**D**), and the number of FLAG-ENL puncta (**E**) in each nucleus in human CD34$^+$ HSPCs. Error bars represent mean ± SEM. *P* values using unpaired, two-tailed Student's *t*-test. **F,** RT-qPCR analysis showing mRNA expression of *HOXA9/10* in human CD34$^+$ HSPCs expressing indicated FLAG-*ENL* transgenes. Error bars represent mean ± SEM (n = 3). **G,** Quantification of colonies formed by human CD34$^+$ HSPCs expressing indicated FLAG-*ENL* transgenes. Error bars represent mean ± SEM (n = 3). *P* value using unpaired, two-tailed Student's *t*-test.

242

Supplementary Figure S18

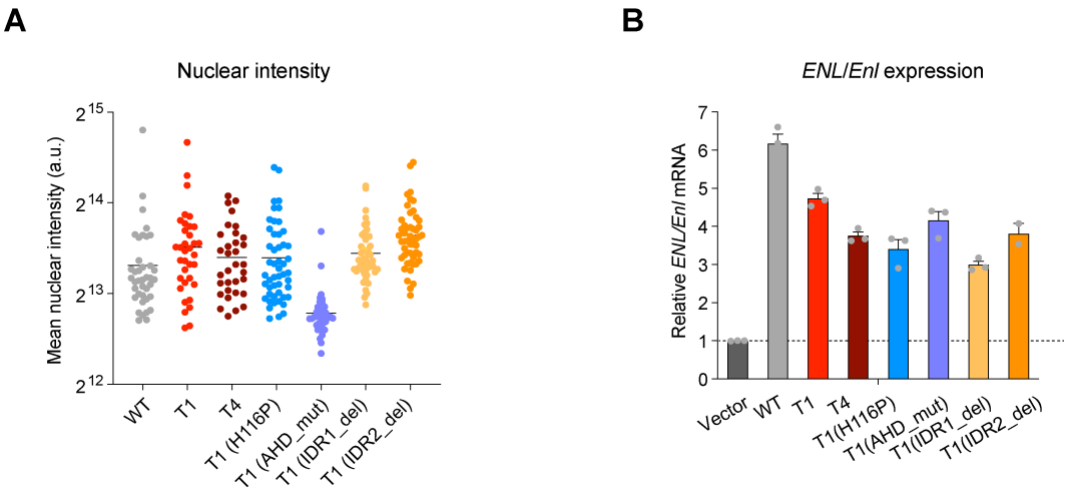

Supplementary Figure S18. Expression levels of different FLAG-*ENL* transgenes in LSK cells. A, Mean nuclear intensity of indicated FLAG-ENL proteins based on anti-FLAG IF staining in LSK cells. Line indicates mean value. **B,** RT-qPCR analysis showing total mRNA levels of human and mouse *ENL/Enl* in LSK cells expressing empty vector or indicated human FLAG-*ENL* transgenes. The primers used for RT-qPCR can detect both human and mouse *ENL/Enl*. Error bars represent mean ± SEM (n = 3).

Supplementary Figure S19

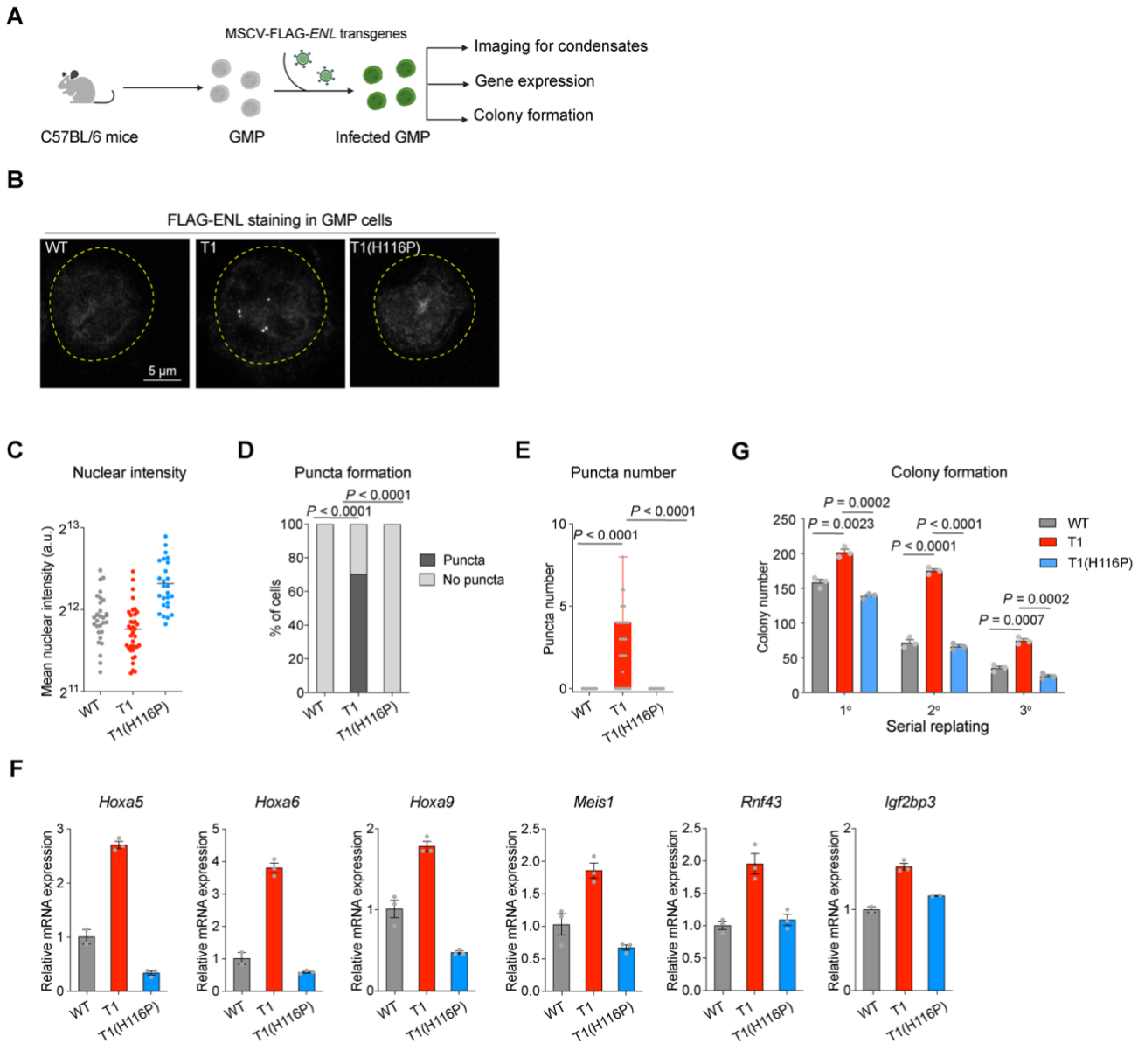

Supplementary Figure S19. Condensate formation property correlates with mutant ENL's oncogenic function in GMP cells. A, Schematic representation of the transduction of various FLAG-tagged *ENL* transgenes in GMP cells and subsequent experiments (shown in **B**-**G**). **B,** Representative images of anti-FLAG IF staining in GMP cells expressing indicated FLAG-*ENL* transgenes. **C**-**E,** Nuclear intensity (**C**), percentage of nuclei with or without FLAG-ENL puncta (**D**), and the number of FLAG-ENL puncta (**E**) in each nucleus in GMP cells. Error bars represent mean ± SEM. *P* values using unpaired, two-tailed Student's *t*-test. **F,** RT-qPCR analysis showing mRNA expression of *Hoxa5/6/9*, *Meis1*, *Rnf43*, *Igf2bp3* in GMP cells expressing indicated FLAG-*ENL* transgenes. Error bars represent mean ± SEM (n = 3). **G,** Quantification of colonies formed by GMP cells expressing indicated FLAG-*ENL* transgenes. Error bars represent mean ± SEM (n = 3). *P* value using unpaired, two-tailed Student's *t*-test.

249

Supplementary Figure S20

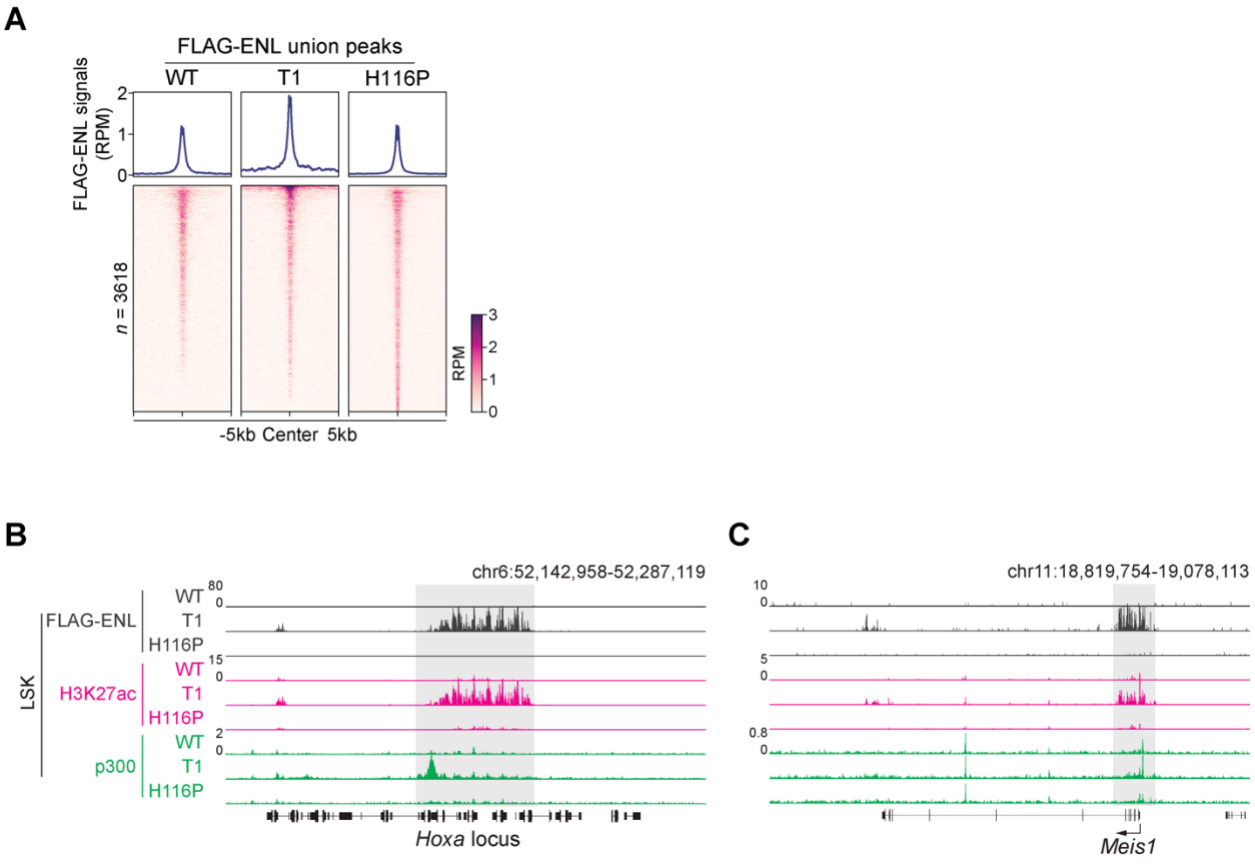

Supplementary Figure S20. Disrupting condensate formation by the H116P mutation reduces ENL-T1-induced increases in chromatin occupancy of FLAG-*ENL*, H3K27ac, and p300 at a subset of target genes. A, Average occupancies (top) and heatmap (bottom) representation of FLAG-ENL-bound peak regions in LSK cells expressing the indicated FLAG-*ENL* transgenes. The CUT&Tag signals are normalized by reads per million (RPM). See Supplementary Table S31. **B, C,** Genome browser view of FLAG-ENL, H3K27ac, and p300 CUT&Tag or ChIP-seq signals at *Hoxa* (**B**) and *Meis1* (**C**) gene loci in LSK cells expressing the indicated FLAG-*ENL* transgenes.

Supplementary Figure S21

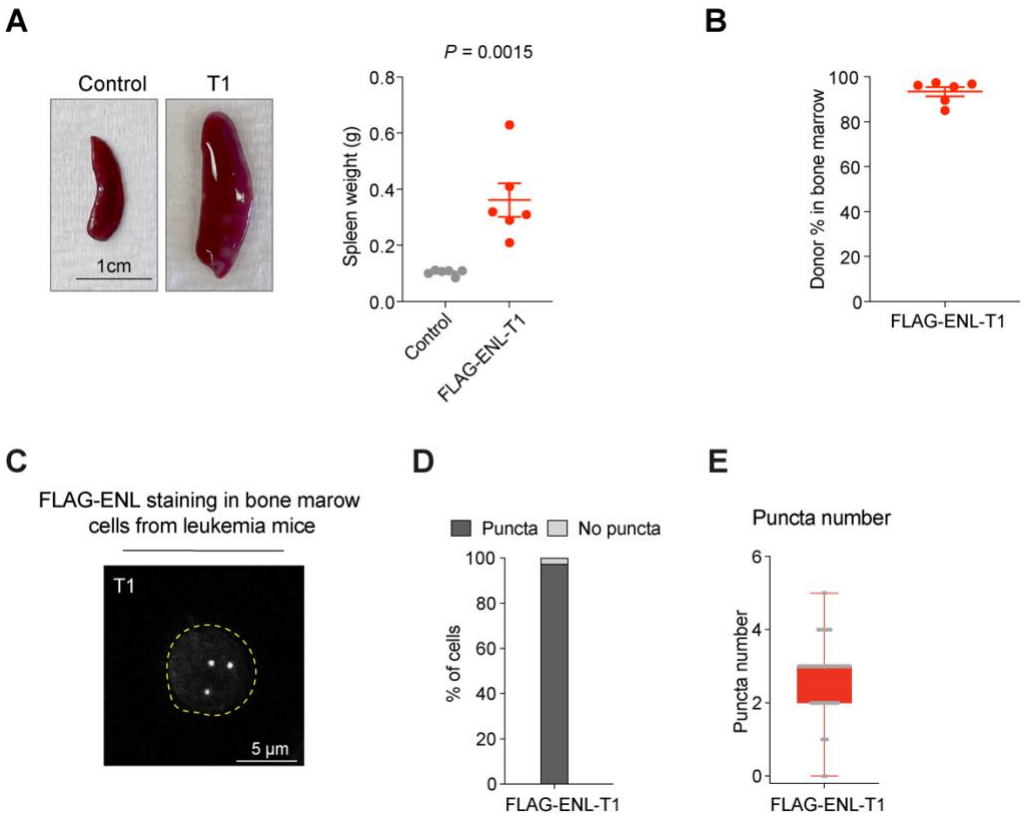

Supplementary Figure S21. Impact of mutant ENL on leukemia development and condensate formation. A, Representative images (left) and weight quantification (right) of spleen harvested from C57BL/6 recipient mice received LSK cells expressing the FLAG-*ENL*-T1 transgenes. Control, the age- and sex-matched C57BL/6 mice. Scale bar, 1 cm; Bars represent the median (n = 6). P value using unpaired, two-tailed Student's t-test. **B,** Flow cytometric quantification of FLAG-*ENL*-T1 expressing cells ($CD45.2^+CD45.1^-$) in the bone marrow harvested at terminal time points from C57BL/6 recipient mice. Bars represent the median (n = 6). **C,** Representative images of anti-FLAG IF staining in cells harvested from C57BL/6 recipient mice that received LSK cells expressing the FLAG-*ENL*-T1 transgene. **D, E,** Percentage of nuclei with or without FLAG-ENL puncta (**D**), and the number of FLAG-ENL puncta (**E**) in each nucleus in cells harvested from C57BL/6 recipient mice that received LSK cells expressing the FLAG-*ENL*-T1 transgene. Error bars represent mean ± SEM. P values using unpaired, two-tailed Student's t-test.

Supplementary Figure S22

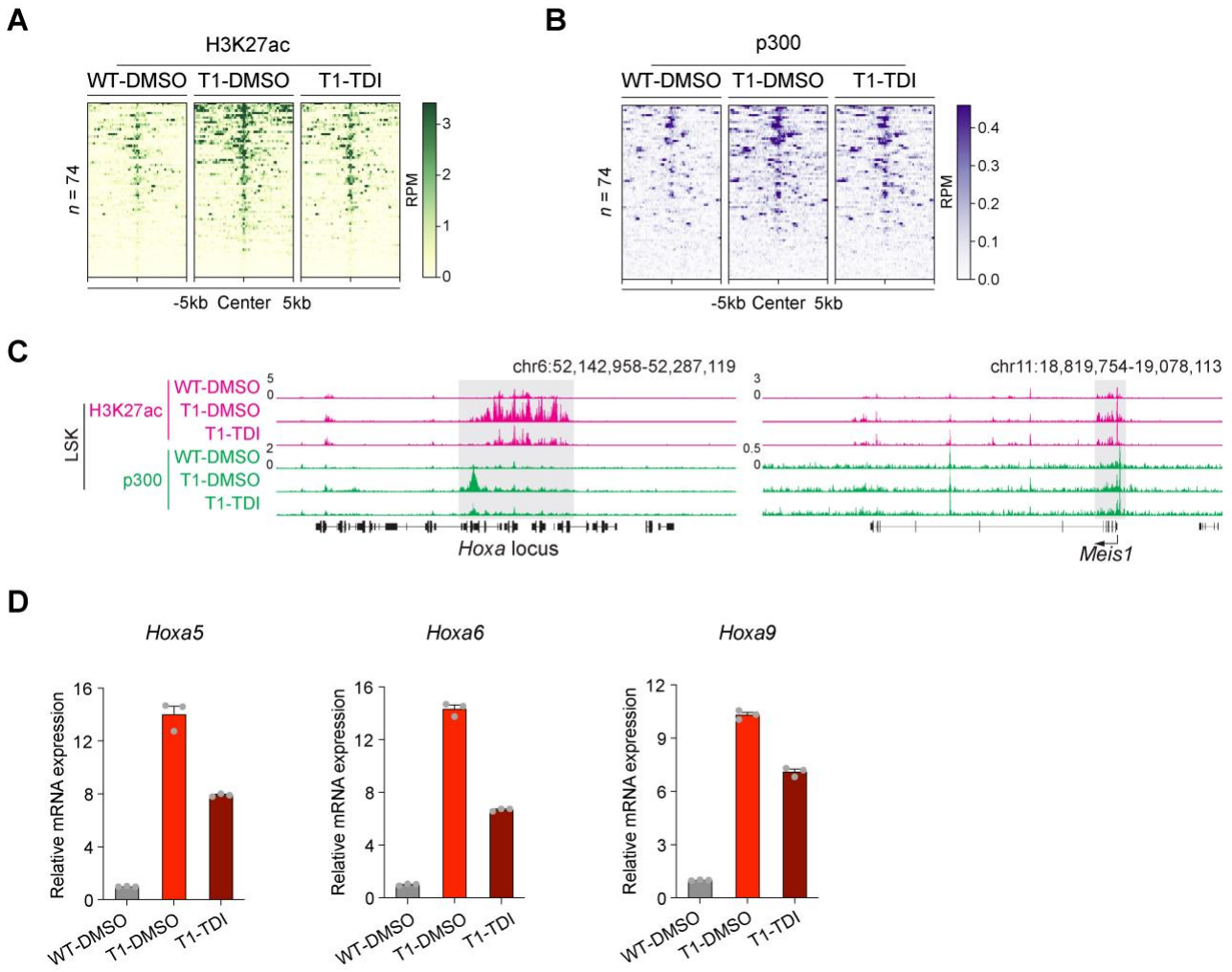

Supplementary Figure S22. Small molecule inhibition of the acetyl-binding activity of mutant ENL suppresses chromatin function and *Hoxa* cluster gene activation in LSK cells. A, B, Heatmap showing H3K27ac (**A**) and p300 (**B**) at genomic regions that exhibit T1-induced increases in FLAG-*ENL* and H3K27ac occupancies in LSK cells expressing indicated FLAG-ENL variants under DMSO or TDI-11055 treatment. See Supplementary Table S33. **C,** Genome browser view of H3K27ac and p300 signals at selected genes (*Hoxa* locus, *Meis1*) under DMSO and TDI-11055 treatment conditions in LSK cells expressing indicated FLAG-ENL variants. **D,** RT-qPCR analysis showing mRNA expression of *Hoxa5/6/9* in LSK cells expressing indicated FLAG-ENL variants under DMSO or TDI-11055 treatment. Error bars represent mean ± SEM (n = 3).

Supplementary Figure S23

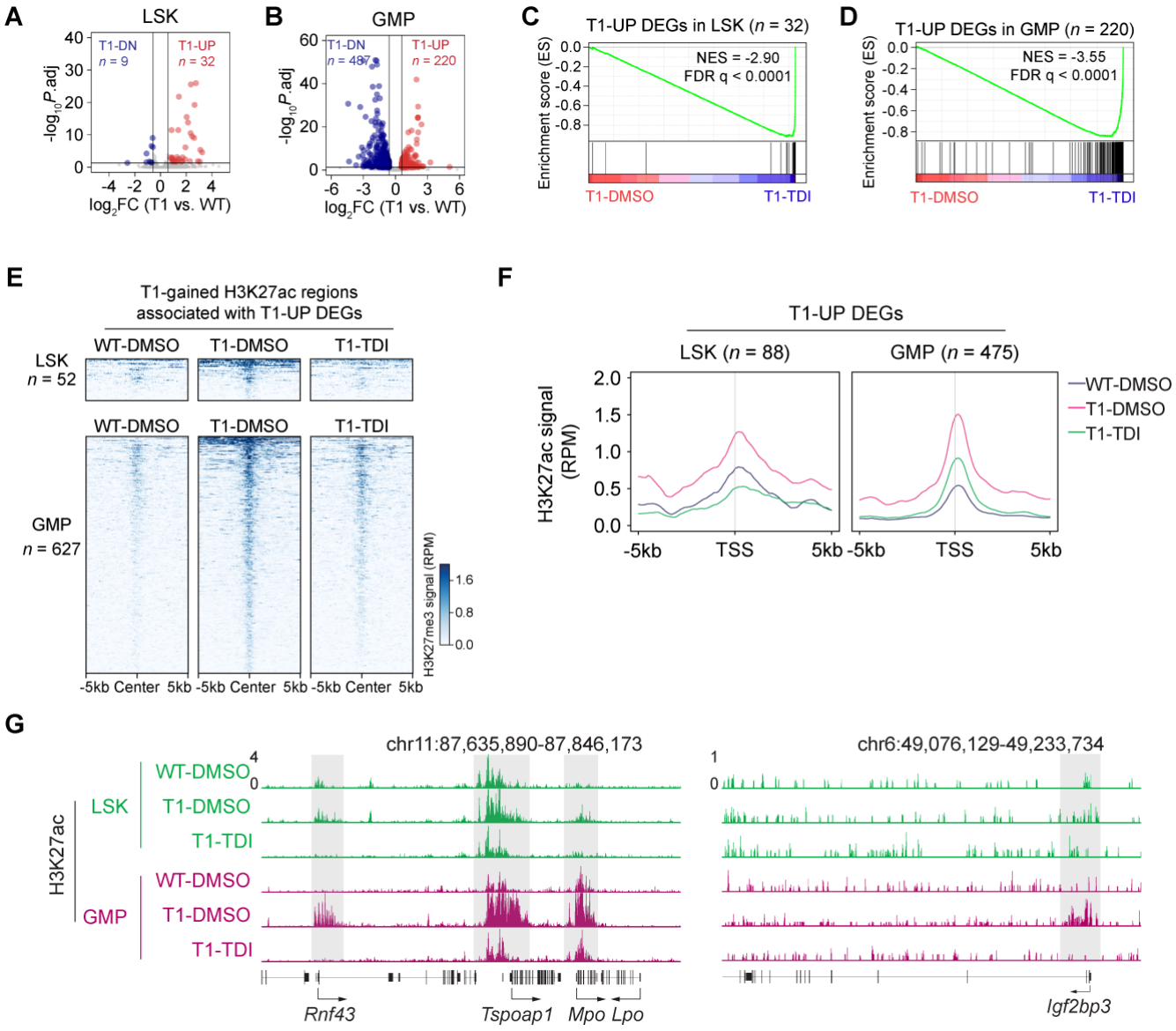

Supplementary Figure S23. Small molecule inhibition of the acetyl-binding activity of mutant ENL impairs its chromatin and transcriptional function in HSPCs. A, **B,** Volcano plots showing the DEGs between *Enl*-WT and T1 under DMSO treatment (see workflow in **Fig. 6L**) in LSK (**A**) and GMP (**B**) cells. T1-UP and DN DEGs are highlighted in red and blue, respectively. FC, fold change; *P*.adj, adjusted *P*-value. See Supplementary Tables S34 and S35. **C**, **D,** GSEA plots evaluating transcriptional changes in *Enl*-T1 LSK (**C**) and GMP (**D**) upon TDI-11055 treatment (10 μM for 48 hours) with T1-UP DEGs identified in LSK (**A**) and GMP (**B**). FDR, false discovery rate; NES, normalized enrichment score. **E,** Heatmap showing H3K27ac signals on T1-gained H3K27ac DRs associated with T1-UP DEGs in LSK (top) and GMP (bottom) under DMSO or 10 μM TDI-11055 treatment conditions (see schematic in **Fig.6P**). **F,** Average occupancies of H3K27ac on the promoters of T1-UP DEGs in LSK (left) and GMP (right) under DMSO or 10 μM TDI-11055 treatment conditions (see schematic in **Fig.6P**). TSS, transcriptional start site. **G,** Genome browser view of H3K27ac CUT&Tag signals at selected genes (*Rnf43*, *Tspoap1*, *Mpo*, *Igf2bp3*) under DMSO and TDI-11055 treatment conditions in LSK and GMP.

283

Supplementary Figure S24

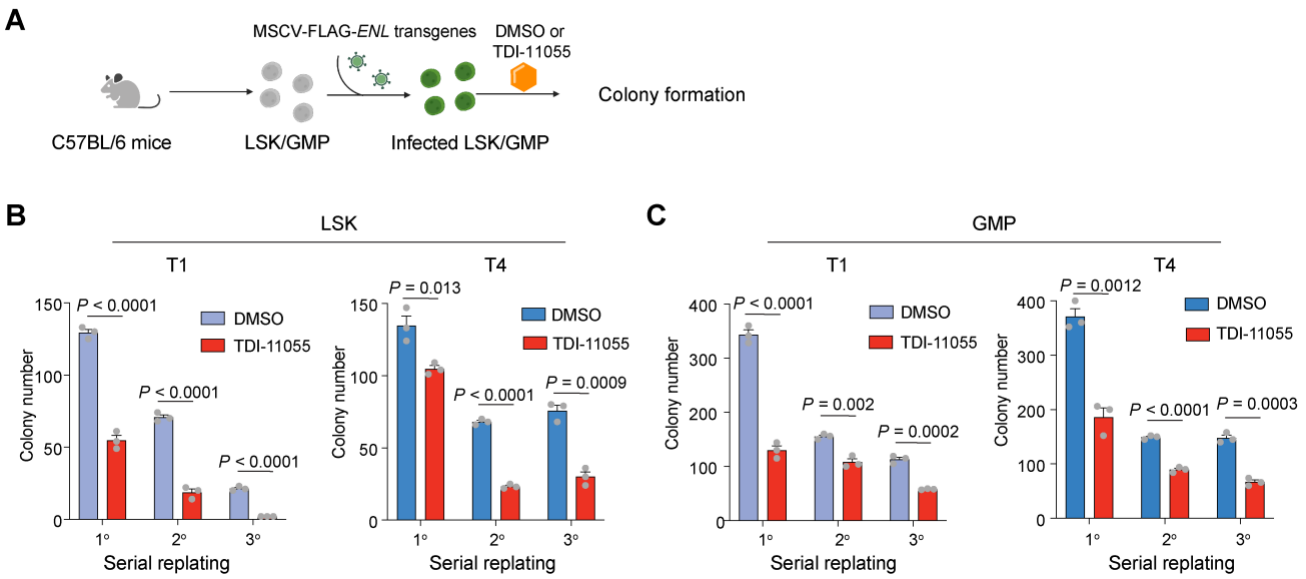

Supplementary Figure S24. Small molecule inhibition of the acetyl-binding activity of mutant ENL inhibits its impact on the self-renewal property in HSPCs. A, Schematic representation of transduction of FLAG-*ENL* transgenes in LSK or GMP cells and subsequent experiments. **B, C,** Quantification of colonies formed by LSK (**B**) and GMP (**C**) cells expressing indicated FLAG-*ENL* transgenes under the treatment of DMSO or TDI (1μM). Error bars represent mean ± SEM (n = 3). *P* values using unpaired, two-tailed Student's *t*-test.